T regulatory cells mediate specific suppression by depleting peptide-MHC class II from dendritic cells

Billur Akkaya[1,8,*], **Yoshihiro Oya**[1,2,8], **Munir Akkaya**[3], **Jafar Al Souz**[1], **Amanda H. Holstein**[1,6], **Olena Kamenyeva**[4], **Juraj Kabat**[4], **Ryutaro Matsumura**[2], **David W. Dorward**[5], **Deborah D. Glass**[1,7], and **Ethan M. Shevach**[1,*]

[1]Laboratory of Immune System Biology, National Institute of Allergy and Infectious Diseases, National Institutes of Health, Bethesda, MD 20892, USA

[2]Department of Rheumatology, Allergy & Clinical Immunology, National Hospital Organization Chiba-East National Hospital, Chiba, Japan

[3]Laboratory of Immunogenetics National Institute of Allergy and Infectious Diseases, National Institutes of Health, Rockville, MD 20852, USA

[4]Research Technologies Branch, National Institute of Allergy and Infectious Diseases, National Institutes of Health, Bethesda, MD 20892, USA

[5]Research Technologies Branch, National Institute of Allergy and Infectious Diseases, National Institutes of Health, Rocky Mountain Labs, Hamilton, MT 59840, USA

[6]Present address: University of South Florida Morsani College of Medicine, Tampa, FL 33612, USA

[7]Present address: Rapa Therapeutics, Rockville, MD 20852, USA

[8]These authors contributed equally

Abstract

T regulatory cells (T$_{regs}$) can activate multiple suppressive mechanisms in vitro upon activation via the T cell receptor resulting in antigen-independent suppression. However, it remains unclear whether similar pathways operate in vivo. Here, we found that antigen-specific T$_{regs}$ activated by dendritic cells (DCs) pulsed with two antigens suppressed T$_{naive}$ specific for both cognate and non-cognate antigens in vitro, but only suppressed T$_{naive}$ specific for cognate antigen in vivo. Antigen-specific T$_{regs}$ formed strong interactions with DC resulting in selective inhibition of the

*Address correspondence to Ethan M. Shevach (eshevach@niaid.nih.gov) or Billur Akkaya (billur.akkaya@nih.gov). NIH/NIAID/ LISB, 9000 Rockville Pike, Bethesda, MD 20892, USA. Phone: (301) 496-6449; Fax: (301) 480-7352.

Data availability

The data that support the findings of this study are available from the corresponding author upon request.

binding of T_{naive} to cognate antigen, yet allowing bystander T_{naive} access. Strong binding resulted in removal of the cognate peptide-MHCII (pMHCII) from the DC surface reducing the capacity of the DC to present antigen. The enhanced binding of T_{regs} to DC coupled with their capacity to deplete pMHCII represents a novel pathway for T_{reg}-mediated suppression and may be a mechanism by which T_{regs} maintain immune homeostasis.

Foxp3[+] T regulatory cells (T_{regs}) are critical for the maintenance of immune homeostasis. One of the major unresolved issues regarding their function is whether they can mediate antigen-specific suppression. Several early in vivo studies on T_{regs} suggested a role for antigen specificity in that CD4^{+} T cells from mice lacking the target organ were poor suppressors of disease in those organs[1–7]. Although these studies indicate the importance of antigen mediated priming of T_{regs}, they did not examine whether antigen recognition by T_{regs} had any further role in suppression in vivo. Several mechanisms have been proposed for the T_{reg}-mediated suppression that can target both $T_{effector}$ cell function and antigen presentation. These include: production of tolerogenic molecules [2, 3, 4, 5], consumption of IL-2 [6], CTLA-4 mediated inhibition of costimulation [7, 8], and contact-dependent killing of antigen presentation through Granzyme and perforin [9]. All of these mechanisms are compatible with the paradigm of bystander suppression as suggested by the studies that T_{regs} primed by one antigen could subsequently suppress T cell proliferative responses to other unrelated antigens activated in the same culture [10, 11]. However, these potential mechanisms for T_{reg} suppression have been primarily derived from in vitro studies and the mechanisms of in vivo regulation are likely to be much more complex. Studies examining T_{reg}-dendritic cell (DC) interactions using intravital microscopy demonstrated that antigen-specific T_{regs} specifically interact with DCs and disrupt their stable contact with antigen-specific T cells via unelucidated mechanisms [12, 13].

Here we aimed to analyze the fine specificity of antigen-specific T_{reg}-mediated inhibition of priming naive T conventional (T_{naive}) cells in vivo and to compare the results with antigen-specific T_{reg}-mediated suppression in vitro. To do so, we used both in vitro differentiated antigen-specific induced T_{regs} (iT_{regs}) as well freshly isolated thymic-derived Tregs (tT_{regs}) from T cell receptor (TCR) transgenic mice. To determine the antigen specificity of Treg-mediated suppression in vitro and in vivo, we stimulated the T_{regs} with DCs simultaneously pulsed with two distinct antigenic peptides and examined the expansion of antigen-specific T_{naive} cells. In line with previous observations[11], antigen-specific T_{regs} following activation by double-pulsed DC were capable of suppressing the expansion of T_{naive} specific for their cognate antigen as well as T_{naive} specific for an unrelated antigen in vitro. In contrast, when similar cell populations were transferred in vivo, T_{regs} activated by double-pulsed DC could only suppress T_{naive} specific for their cognate antigen. To explore the mechanisms leading to antigen-specific suppression in vivo, we performed an in depth analysis of the physical interactions of antigen-specific T_{regs} with DCs in comparison to that of antigen-specific T_{naive} cells and demonstrated that T_{regs} acquire a distinct morphology upon contact with DC displaying wider membrane fusion sites, longer contact durations, and bigger clusters in vitro and in vivo. When we sequentially treated DCs with T_{regs} and T_{naive}, T_{regs} that recognized the same antigen as the T_{naive} selectively excluded the T_{naive}. However, T_{reg} pretreatment of double pulsed DCs in vitro disabled the capacity of the DCs to activate

$T_{naïve}$ specific for the antigen recognized by the T_{reg}, but not the response of $T_{naïve}$ specific for an unrelated antigen expressed on the same DC surface. These findings suggested that T_{regs} use suppressor mechanisms in addition to preventing access of T_{naive} to antigen expressed on the DC surface. We demonstrated that antigen-specific T_{regs} remove pMHCII complexes from the DC surface and thereby decrease the capacity of the DCs to present antigen. Most importantly, the removal of pMHCII complexes was antigen-specific as T_{regs} only captured the pMHCII complexes that they recognize, but not any unrelated antigen expressed on the same DC.

Taken together, we describe a novel pathway for antigen-specific T_{reg}-mediated suppression. It first requires a strong interaction of the antigen-specific T_{reg} with the DC presenting its cognate antigen and secondarily removal of the cognate pMHCII from the DC surface in a TCR-specific fashion.

RESULTS

Antigen-specific T_{regs} mediate antigen-specific suppression in vivo

To determine if antigen-specific iT_{regs} exhibit bystander suppression, we generated antigen-specific iT_{regs} using $CD4^+Foxp3^-$ T cells from from OT-II mice. OT-II iT_{regs} markedly suppressed the proliferation of OT-II T cells stimulated with $OVA_{323-339}$ pulsed DCs in vitro, but had only a minimal effect on the proliferation of SMARTA T cells stimulated with DC pulsed with LCMV GP_{61-80} (Supplementary Fig. 1a, b). Similarly, SMARTA iT_{regs} completely suppressed the response of SMARTA T cells to GP_{61-80}-pulsed DCs, but had no effect on the response of OT-II T cells to OVA-pulsed DCs (Supplementary Fig. 1c, d). The failure of OT-II iT_{regs} to suppress the response of SMARTA T cells could be secondary to the requirement that iT_{regs} be re-stimulated in culture to exert their suppressive function. To clarify this point, we co-cultured OT-II and SMARTA T cells in the presence of OT-II iT_{regs} and a mixture of DCs pulsed with $OVA_{323-339}$ and DCs pulsed with GP_{61-80} or with DCs simultaneously pulsed with the OVA and GP. Under both of these activation conditions antigen-specific iT_{regs} suppressed the proliferation of OT-II and SMARTA T cells (Supplementary Fig. 1e, f). This result is similar to previous observations[10] with antigen-specific T_{regs} isolated from TCR transgenic mice. One difference between the studies is that the iT_{regs} required re-stimulation with their cognate antigen even though they were previously activated in culture.

To evaluate whether activated antigen-specific iT_{regs} could also suppress the response to unrelated antigens in vivo, we developed a model in which peptide-pulsed DCs, antigen-specific T cells and antigen-specific iT_{regs} are transferred i.v. to immunocompetent syngeneic recipients. To determine whether antigen-specific iT_{regs} activated with their cognate antigen could suppress responses of a second antigen-specific T cell population when stimulated with both their cognate antigen and the unrelated antigen, we first co-transferred OT-II and SMARTA T cells, OT-II iT_{regs}, and separate populations of DCs pulsed with $OVA_{323-339}$ or GP_{61-80}. OT-II iT_{regs} completely suppressed the response of OT-II T cells, but failed to suppress the response of SMARTA T cells. Similarly, when SMARTA iT_{regs} were transferred with OT-II and SMARTA T cells and separate populations of pulsed DCs, they completely suppressed the proliferation of SMARTA T cells, but had no

effect on the proliferation of OT-II T cells (Fig. 1a). To determine whether antigen-specific iT_{regs} activated with their cognate antigen could suppress responses of a second antigen-specific T cell population in the same environment when stimulated with DCs pulsed with both peptides, we co-transferred OT-II and SMARTA T cells, OT-II iT_{regs}, and DCs simultaneously pulsed with $OVA_{323-339}$ and GP_{61-80} peptides. OT-II iT_{regs} completely suppressed the response of OT-II T cells and only slightly suppressed the response of SMARTA T cells. Likewise, when SMARTA iT_{regs} were transferred with OT-II and SMARTA T cells and double-pulsed DCs, they completely suppressed the proliferation of SMARTA T cells, but had no effect on the proliferation of OT-II T cells (Fig. 1b). Similar to iT_{regs}, antigen-specific T_{regs} from TCR transgenic mice that were expanded in vitro via plate bound anti-CD3, anti-CD28, and IL-2 or in vivo via IL-2-anti-IL-2 complex treatment also displayed antigen specific suppression when adoptively transferred in vivo (Supplementary Fig. 2a-c).

The ability of antigen-specific T_{regs} to suppress responses to their cognate antigen expressed on DCs, but not to suppress responses to a second antigen expressed on the same DC population, strongly suggested that T_{reg} suppressor mechanisms involving the down-regulation of costimulatory function on DC or suppressor cytokines played little to no role in iT_{reg} suppression in vivo. To test this possibility, we made use of TCR transgenic strains specific for pigeon cytochrome C (PCC) on a $Rag2^{-/-}$ background that were either deficient for CTLA-4 or IL-10. Because these mice lacked a normal TCR repertoire, they were phenotypically normal and exhibited no signs of T cell activation or autoimmune disease. PCC-specific iT_{regs} generated from either $Il10^{-/-}$ or $Ctla4^{-/-}$ animals were as suppressive as PCC-specific iT_{regs} generated from 5CC7 TCR transgenic $Rag2^{-/-}$ donors (Fig. 1c, d) strongly suggesting that neither IL-10 nor CTLA-4 played a major component in iT_{reg} suppressor function in vivo.

Antigen-specific iT_{regs} engage in intense and unique interactions with antigen-pulsed DCs

As an initial approach to determine the mechanism of antigen-specific suppression in vivo, we characterized the interactions of freshly isolated 5CC7 T_{naive}, 5CC7 $T_{activated}$ and 5CC7 iT_{reg} with MCC_{88-103} pulsed DCs using SEM and TEM after 2 h of co-culture in vitro. We quantified the number of T cells per DC for a total of 40 DCs using SEM images and found a significantly higher number of iT_{reg} bound per DC (Fig. 2a, b). Tilted SEM images of the T-DC binding sites revealed an average of 3–9 membrane fusion nanodomains per T-DC couple. Membrane fusion nanodomains have been reported to contain clusters of TCR and co-receptors [14, 15, 16, 17]. Length measurements of nanodomains visible in random, representative micrographs showed that iT_{regs} displayed significantly wider nanodomains compared to nanodomains formed by T_{naive} or $T_{activated}$ suggesting a more mature contact (Fig. 2c, d).

TEM images of T-DC couples demonstrated that upon binding to DC, iT_{reg} exhibited a morphology distinct from DC-bound $T_{activated}$, with uropods at the rear end and finger-like projections at the leading edge. iT_{reg}-DC contact sites contained filopodia that were not observed at $T_{activated}$-DC interaction sites (Fig. 2e). We also detected by live confocal microscopy that OT-II iT_{regs}, but not OT-II $T_{activated}$ displayed prominent amoeboid

movements with highly dynamic filopodial protrusions and contractions at the DC binding site which increased the volume of interaction with the antigen-pulsed DCs (Fig. 2f, Supplementary video 1, 2a, b).

We then characterized the real-time interactions of iT_{regs} and $T_{activated}$ with DCs in vivo by co-transferring OT-II iT_{regs} or OT-II $T_{activated}$ with antigen-pulsed DCs into WT mice (Fig. 3a). DCs that were pulsed with $OVA_{323-339}$ were directed to popliteal lymph nodes by injection into the footpad to facilitate interactions with either OT-II iT_{reg} or OT-II $T_{activated}$ that were simultaneously injected intravenously. We visualized the lymph nodes by intravital two photon microscopy at 18–20 h post-transfer and found that OT-II iT_{regs} formed larger clusters around the DCs, whereas OT-II $T_{activated}$ were found more remotely located (Fig. 3b). OT-II iT_{regs} engaged in more intense interactions with DC as quantified by the greater volume of contact and longer contact durations recapitulating our in vitro observations in vivo (Fig. 3c, Supplementary video 3a, b).

One possible explanation for antigen-specific suppression in vivo (Fig. 1a, b) is that the greater avidity of the iT_{regs} for the antigen-pulsed DCs inhibits the access of naive antigen-specific T cells. To address whether antigen-specific competition exists in vivo, we transferred OT-II T_{naive} with OT-II iT_{regs} or with OT-II $T_{activated}$. The dynamic movement and localization of OT-II T_{naive} were visualized by intravital two-photon microscopy 18–20 h post-transfer. Intravital microscopy showed that in the presence of cognate antigen, OT-II T_{naive} exhibited slower movement and enhanced clustering around the DCs. The presence of OT-II $T_{activated}$ resulted in some degree of increased mobility and reduced clustering around the DC of the co-transferred OT-II T_{naive}. In contrast, in the presence of OT-II iT_{regs}, OT-II T_{naive} exhibited significantly greater mobility as reflected by larger increases in average T cell track velocities and longer distances to the closest DC than in the presence of OT-II $T_{activated}$ (Fig. 3 d, e; Supplementary video 4 a-d). In parallel studies of T cell proliferation in vivo at 72h after transfer, only modest inhibition of proliferation of OT-II T_{naive} was seen in the presence of OT-II $T_{activated}$, while profound inhibition of the proliferation of OT-II T_{naive} was observed in the presence of OT-II iT_{regs} (Fig. 3f, g). Taken together, these microscopic studies demonstrate that the profound inhibition of T cell proliferation by the antigen-specific iT_{regs} is consistent with the intense contact between T_{regs} and DCs.

Visualization of T_{reg}-mediated antigen-specific suppression in vivo

To further analyze the mechanism of suppression mediated by antigen-specific iT_{regs}, we adoptively transferred DCs pulsed with both $OVA_{323-339}$ and GP_{61-80} peptides into WT animals via the footpad. We then co-transferred OT-II or SMARTA iT_{regs} with a mixture of OT-II and SMARTA T_{naive} i.v. to visualize how real-time interactions between DC and antigen-specific T_{naive} and bystander T_{naive} are regulated by iT_{regs}. We extracted the lymph nodes 18–20 h post-transfer and sectioned them in ice-cold PBS to preserve the microarchitecture of the lymph node as well as the viability of cells. After warming sections to 37 °C to restore cell movement, we tracked the cells for up to 12 h. We found that the presence of OT-II iT_{regs} led to selective exclusion of OT-II T_{naive} and SMARTA iT_{regs} led to selective exclusion of SMARTA T_{naive} from DC contact. In contrast, bystander $CD4^+$ T cells maintained their interaction with DCs (Fig. 4a, Supplementary video 5). Regardless of the

antigen dose, antigen specific T_{naive} cells moved at higher speeds and interacted for shorter times than bystander T_{naive} cells, indicating that the T_{reg}-mediated disruption of stable contacts was antigen-specific (Fig. 4b-d).

To visualize the morphological changes that occur in vivo during T cell activation, we transferred $OVA_{323-339}$ and GP_{61-80} double pulsed DCs, OT-II and SMARTA T_{naive} cells with OT-II or SMARTA iT_{regs} to normal recipients. We then performed confocal microscopy of whole popliteal lymph node sections 24 h post-transfer. In the absence of T_{regs}, OT-II T cells were found enlarged in size as a morphological sign of activation. The volume of the OT-II T cell blasts was significantly decreased in the presence of OT-II, but not SMARTA iT_{regs}, indicating that the inhibition of T cell blasting is antigen-specific (Fig. 4e, f). Furthermore, the OT-II T cells retained the spherical morphology of unstimulated T cells only in the presence of OT-II iT_{regs} (Fig. 4f), but not SMARTA iT_{regs}. These findings confirm, at the morphological level, that antigen-specific iT_{regs} do not mediate bystander inhibition in vivo.

T_{regs} acquire peptide-MHC II complexes by capturing DC membrane fragments

The data presented above are compatible with a model in which the major inhibitory function of antigen-specific iT_{regs} is to prevent the access of T_{naive} to the pMHCII complex on the DC surface in a competitive fashion. If this is the case, removal of the iT_{regs} from co-cultures in vitro should abolish their suppressive effects. To test this, we pre-cultured the iT_{regs} with DCs pulsed with both $OVA_{323-339}$ and GP_{61-80} peptides. We then depleted the iT_{regs} from the DCs, and evaluated the capacity of the treated DCs to stimulate TCR transgenic T_{naive} cells. DCs pre-cultured with OT-II iT_{regs} failed to activate OT-II T cells, but retained the capacity to activate SMARTA T cells. Similarly, DCs pre-cultured with SMARTA iT_{regs} failed to activate SMARTA T cells, but stimulated OT-II T cells as efficiently as control DCs (Fig. 5a, b). Furthermore, when we added fresh peptide to DCs pre-cultured with iT_{regs}, the antigen presentation capacity of the DCs could be restored (Fig. 5c, d). These results strongly suggest that, antigen-specific iT_{regs} can decrease the capacity of DCs to present their cognate antigen, but leave intact the presentation of antigens not recognized by their TCR.

We hypothesized that the intense interaction of iT_{regs} with the DCs might result in the removal of pMHCII complexes from the DC surface. To evaluate whether iT_{regs} acquire DC-derived membrane complexes by a process of trogocytosis, we labeled DC membrane with the lipophilic dye PKH-26 and pulsed with MCC_{88-103}. The DCs were then cultured with 5CC7 T_{naive}, $T_{activated}$, or iT_{regs} for 18 h. 5CC7 iT_{regs} acquired a greater amount of the DC membrane than T_{naive} or $T_{activated}$ as measured by the increase in their PKH-26 fluorescence intensity (Fig. 6a). We then tested whether the iT_{regs} acquire multiple membrane antigens from the DC surface. Indeed, when we stained the antigen-specific iT_{regs}, we could easily detect surface molecules involved in the immune synapse such as MHCII, CD86, ICOS-L, and PD-L2 (Supplementary Fig. 3a). It is very likely that these antigens were derived from the surface of the DC as they could not be detected on the surface of the iT_{regs} either prior to the co-culture or after polyclonal activation with plate-bound anti-CD3 and anti-CD28 in the absence of DC (Supplementary Fig. 3b).

To visualize the membrane patches containing total MHCII acquired by the antigen-specific iT$_{regs}$, we fixed co-cultures of OVA$_{323-339}$-pulsed DCs with OT-II T$_{naive}$, T$_{activated}$, or iT$_{regs}$ after 3h and imaged by confocal microscopy. In order to distinguish between the isolated membrane patches separated from DCs and the actual DC-T cell contact sites, we performed 3D reconstruction of DCs and used it to mask other channels to eliminate signal coming from DCs. Using masked channels, we created 3D surfaces for the T cells and T$_{regs}$ and quantitated the mean intensity of the acquired MHCII (Fig. 6b). The MHCII acquired by iT$_{regs}$ had greater intensity than those in T$_{activated}$ (Fig. 6c). Altogether these findings suggest that antigen-specific T$_{regs}$ have higher trogocytic capacity than T$_{activated}$ cells.

Antigen-specific iT$_{regs}$ downregulate antigen-presentation by DC by removing pMHCII complexes from the DC surface

Although confocal microscopy was sensitive enough to detect the total MHCII signal, its sensitivity was not adequate to visualize the acquisition of antigen-specific pMHCII complexes. We then used TEM to visualize and quantify the acquisition of antigen-specific pMHCII early during T-DC interaction. We made use of a monoclonal antibody, D4, which detects complexes of MCC$_{(88-103)}$-I-E^k [18]. We cultured MCC$_{88-103}$ pulsed DCs with either 5CC7 T$_{naive}$, T$_{activated}$ or iT$_{regs}$ for 3 h and stained with biotinylated D4 antibody followed by streptavidin conjugated quantum dots and imaged by TEM. Only iT$_{regs}$ had intense DC contacts in which they engulfed parts of the DC membrane (Fig. 6d). More importantly, we only observed transfer of quantum dots to iT$_{regs}$ and not to T$_{naive}$ or T$_{activated}$ (Fig. 6e). The quantum dots were detected both on the T$_{reg}$ cell surface and within endosomes (Fig. 6f).

To assay whether a similar process of uptake of DC membranes by iT$_{regs}$ occurred in vivo, we adoptively transferred MCC$_{88-103}$ pulsed DCs via the footpad and simultaneously transferred 5CC7 T$_{naive}$, T$_{activated}$, or iT$_{regs}$ into wild-type B10.A animals. Internalized MCC$_{88-103}$-I-E^k complexes were found in 5CC7 iT$_{regs}$ on day 3 post-transfer in the draining popliteal lymph node, whereas no complexes could be detected in 5CC7 T$_{naive}$ or T$_{activated}$ indicating that antigen-specific iT$_{regs}$ indeed captured and retained cognate pMHCII (Fig. 7a).

To further dissect the parameters that governed iT$_{reg}$-mediated uptake of pMHCII complexes, we co-cultured 5CC7 T$_{naive}$, T$_{activated}$, or iT$_{regs}$ for 18 h with freshly isolated splenic DCs that had been pulsed with MCC$_{88-103}$ peptide at different loading doses and measured the amount of MCC$_{88-103}$-I-E^k complexes acquired by T cells using flow cytometry. We detected significantly higher amounts of pMHCII complexes both on the surface and in the intracellular compartment of iT$_{regs}$ than in T$_{naive}$ or T$_{activated}$ at any peptide concentration (Fig. 7b, c). pMHCII complexes on 5CC7 iT$_{regs}$ were detectable by flow cytometry as early as 3 h post-co-culture with greater accumulation over time, whereas they only became detectable on the surface of T$_{activated}$ after 6 h. No pMHCII complexes were shown on the surface of polyclonal iT$_{regs}$ substantiating the role of TCR-pMHCII interactions for acquisition of pMHCII complexes by T$_{regs}$ (Supplementary Fig. 4a, b). The MCC$_{88-103}$-I-E^k level detected on the DC surface was reduced to greater extent in the presence of 5CC7 iT$_{regs}$ than with T$_{naive}$ or T$_{activated}$ (Fig. 7d). This result is consistent with an iT$_{reg}$-mediated depletion of pMHCII from the DC surface. We observed similar results

with T_{regs} isolated from TCR transgenic mice on a *Rag2*$^{+/+}$ background. Both antigen-specific iT_{regs} and T_{regs} (likely tT_{regs}) were able to reduce the DC surface pMHCII to the same degree (Fig. 7e, f).

The interaction of CTLA-4 on the surface of T_{reg} with CD80 or CD86 on the surface of DC has been previously shown to result in the capture of these molecules by the T_{reg} through a process of transendocytosis[8]. To determine if CTLA-4 mediated transendocytosis plays a role in the uptake of MCC_{88-103}-I-E^k or the removal of MCC_{88-103}-I-E^k from the DC surface, we again generated MCC_{88-103} specific iT_{regs} from CTLA-4 deficient 5CC7 TCR transgenic mice and cultured them with MCC_{88-103} pulsed DCs. The uptake of the the MCC_{88-103}-I-E^k complex by wild-type and *Ctla4*$^{-/-}$ iT_{regs} was identical indicating that CTLA-4 did not play a role in the uptake of pMHCII complexes (Supplementary Fig. 5). These findings indicate that antigen-specific T_{regs} capture a critical amount of pMHCII from DC, thus decrease the presentation of cognate antigen without the CTLA-4 mediated mechanisms involved.

Acquisition of pMHCII complexes by T_{regs} is antigen-specific

As T_{regs} manifested their suppressive effect in an antigen-specific manner in vivo, it was important to determine whether the acquisition of pMHCII complexes is limited to cognate pMHCII. To test this, we pulsed DCs from B10.A mice with equimolar amounts of MCC_{88-103} and HEL_{46-61} peptides and co-cultured the pulsed DCs for 18 h with 5CC7 and 3A9 (HEL_{46-61} specific) iT_{regs} or tT_{regs}. 5CC7 T_{regs} acquired MCC_{88-103}-I-E^k complexes, but not HEL_{46-61}-I-A^k complexes (detected with mAb AW3.18 [19]). Similarly, HEL_{46-61}-I-A^k complexes, but not MCC_{88-103}-I-E^k complexes, were captured by 3A9 T_{regs} even though both 5CC7 and 3A9 T_{regs} were capable of interacting with the same DC (Fig. 8a, Supplementary Figure 6). Furthermore, DC levels of pMHCII were depleted in an antigen-specific manner, while the level of the non-cognate complex remained unchanged (Fig. 8b-c, Supplementary Figure 6). Next, we confirmed the functional consequence of antigen restricted pMHCII removal in this particular two antigen system as in Fig. 5 by pre-culturing the iT_{regs} with double pulsed DCs and evaluating the capacity of the treated DCs to stimulate naive TCR transgenic T cells. We observed that DCs pre-cultured with 5CC7 or 3A9 iT_{regs} failed to activate naive T cells specific for the cognate antigen recognized by the antigen-specific iT_{regs}, yet maintained the capacity to activate naive T cells specific for the non-cognate antigen (Supplementary Fig. 7). When antigen specific T_{regs} were transferred in vivo with double pulsed DCs, they only acquired their cognate complexes (Fig. 8d-e, Supplementary Figure 6). Furthermore, double pulsed DCs were found depleted in cognate pMHCII, while the amount of non-cognate complex was unchanged (Fig. 8f, Supplementary Figure 6). Altogether our data confirm that antigen-specific T_{regs} can execute suppressor function by acquiring pMHCII complexes from double pulsed DCs in an antigen-specific manner (Supplementary Figure 8).

DISCUSSION

It is widely accepted that TCR signaling is required to induce the program of activities that mediate T_{reg} suppressor function in an antigen non-specific manner resulting in suppression

of DCs and/or T cells in their vicinity. Here we define the fine specificity of T_{reg}-mediated suppression in a reliable, in vivo assay for suppression of proliferation by antigen-specific T_{naive} cells. When we activated antigen-specific T_{reg} function in vivo with DCs that were simultaneously pulsed with two peptides, suppression was completely antigen-specific.

Previous studies of T_{reg}-DC interactions [12, 13] using antigen-specific T_{regs} from TCR transgenic mice on a conventional background demonstrated that the primary mechanism of suppression used by the T_{regs} was to prevent the formation of stable interactions between the antigen-specific T_{naive} cells and the antigen-bearing DC. The antigen specificity of the inhibition of T_{naive} cell binding to the antigen exposed DC was not addressed. Yan et al. [20] and Chen et al. [21] demonstrated that upon exposure to IL-2 polyclonal T_{regs} form strong adhesive contacts with DCs independent of antigen and MHCII recognition resulting in suppression of the interaction of the DCs with antigen-specific T_{naive} cells. While we observed that T_{regs} inhibited antigen-specific T_{naive} cell interactions with antigen-pulsed DCs, inhibition of the interaction in vivo was antigen-specific. We did not observe any interactions between polyclonal iT_{regs} and DCs even though the iT_{regs} were generated in the presence of IL-2.

We also observed that preincubation of the iT_{regs} in vitro with double pulsed DCs inhibited the subsequent capacity of the DCs to activate T_{naive} specific for their cognate antigen, but not T_{naive} specific for the second antigen expressed on the DC. The defective stimulatory capacity of the iT_{reg}-treated DCs could be restored by re-pulsing the DCs with the cognate peptide. This finding strongly suggested that mere competition for binding is not sufficient to completely explain antigen-specific T_{reg}-mediated suppression.

The strong binding of the iT_{regs} and their capacity to debilitate DC function in an antigen-specific manner raised the possibility that the iT_{regs} were removing their target antigen from the DC surface by a process similar to trogocytosis [22]. The capacity of T cells to take up pMHCII complexes has been known for decades [23, 24, 25]. There are a number of important differences between these earlier studies and our observations. First, the capacity of T cells to take up DC-derived membranes required that the T cells be activated by antigen or mitogens. Once activated, the T cells could acquire membrane molecules in an antigen-independent manner [23, 24]. In our studies, uptake of pMHCII complexes in vivo and in vitro was antigen-specific and the non-cognate antigen could not be detected on or in the antigen-specific T_{regs}. Secondly, iT_{regs} appeared to have a much greater capacity than T_{naive} or $T_{activated}$ to take up pMHCII complexes. Activated antigen-specific T cells took up less pMHCII than T_{naive} cells perhaps because they had downregulated their TCR during stimulation with antigen. Although we specifically examined the uptake of pMHCII complexes using anti-pMHCII mAbs, T_{regs} could take up several other DC-derived molecules including CD86 and PD-L2. It is therefore likely that T_{reg} TCRs exist in a cluster as part of the immune synapse (IS) interacting with their cognate pMHCII together with surrounding DC molecules involved in co-stimulation and cell adhesion, but excluding the non-cognate pMHCII complexes expressed on the same DC. T_{regs} have been shown to form more stable ISs than activated T cells [26] and exclude the protein kinase, PKC-θ, from the IS. As the IS is responsible for endocytosis and degradation of the TCR [15], the unique

properties of the T_{reg} IS may promote the ability of their TCR to bind and take up pMHCII complexes and adhesion/costimulatory molecules from the DC.

The molecular basis for the strong binding of T_{regs} to antigen-pulsed DCs and their subsequent ability to remove membrane complexes from the DC surface remains unknown. Recent studies using phosphoproteomics have identified a set of proteins differentially expressed in T_{regs} that are linked to the cytoskeletal machinery and that may confer unique properties to the T_{reg} IS [27]. Lymphocyte functional antigen-1 (LFA-1) has been shown to promote stable interactions of T_{regs} with DCs [28]. However, blocking LFA-1-ICAM-1 interactions inhibits the binding of both non-T_{regs} and T_{regs} with DCs and has not allowed us to specifically block T_{reg} interactions. A second candidate molecule on the T_{regs} is CTLA-4 whose binding to CD80 and CD86 may also be involved in T_{reg}-DC adhesion in addition to signal transduction [29]. However, CTLA-4 appeared to play no role in our model system either in mediating suppression or capture of antigen from the DC surface. Integrins other than LFA-1 could also play a role in T_{reg}-DC interactions as α4β1 has been shown to co-localize in the synapse and potentially augment T_{reg}-DC binding [30]. Lastly, neuropilin-1 (Nrp1) has been proposed [31] to increase the binding of T_{regs} to DCs and enhance their sensitivity to antigenic signals.

One argument which has been raised against the existence of additional pathways of T_{reg}-mediated suppression is that they would have been discovered in studies of genetic diseases that result in serious autoimmune manifestations similar to mice with deficiencies in Foxp3, CTLA-4 or TGF-β. Genetic defects in the model proposed here involving physiologic interactions of the TCR with pMHCII would lead to a failure to mount any type of immune response and would not be regarded as unique to T_{regs}. However, a subpopulation of activated T_{regs} can be identified in vivo[38–40] and these activated T_{regs} are lost in mice with T_{reg}-specific deletion of the TCR [32, 33]. Deletion of the gene encoding adaptor protein SLP-76 in mature T_{regs} also results in an enhanced naive phenotype and loss of suppressive function [34]. As SLP-76 plays a major role in actin polymerization in T cells [35], loss of SLP-76 may result in impairment of IS formation in T_{regs} and the ability to capture pMHCII complexes. These observations raise the possibility that this subpopulation of activated T_{regs} in vivo is directly mediating suppression via the interaction of their TCR with complexes of self pMHCII resulting in constant removal of self pMHCII complexes from the DC surface. Thus, continuous removal of self pMHCII complexes may be the mechanism by which T_{regs} maintain physiologic immune homeostasis.

MATERIALS AND METHODS

Animals and reagents

C57BL/6NCrl mice were purchased from Charles River (Germantown, MD). DsRed.T3 and Foxp3.RFP mice were purchased from Jackson Laboratory (Bar Harbor, ME). Moth Cytochrome C ($MCC_{88–103}$) specific TCR transgenic 5CC7-FoxP3.GFP $Rag2^{-/-}$, 5CC7-$Ctla4^{-/-}Rag2^{-/-}$, 5CC7-$Il10^{-/-}Rag2^{-/-}$, Hen Egg Lysozyme ($HEL_{46–61}$) specific TCR transgenic 3A9 $Rag2^{-/-}$, $OVA_{323–339}$ specific TCR transgenic OT-II, OT-II-$Rag2^{-/-}$, CD11c.YFP, FoxP3.GFP, B10.A mice were obtained from Taconic Farms (Hudson, NY) under the NIAID contract. Lymphocytic Choriomeningitis Virus Glycoprotein (LCMV

GP_{61-80}) specific TCR transgenic SMARTA mice were originally obtained from the La Jolla Institute of Allergy and Immunology. OT-II-DsRed.T3 mice were generated by a single cross between OT-II and DsRed.T3 mice. 5CC7-FoxP3.GFP $Rag2^{+/+}$, 3A9-FoxP3.GFP $Rag2^{+/+}$ mice were generated by two crosses into B10.A-Foxp3.GFP background. OT-II-Foxp3.RFP mice were generated by a single cross between OT-II and Foxp3.RFP mice. All mice were maintained in National Institutes of Health animal facilities in compliance with Animal Care and Use Committee standards.

Cells were cultured in sterile complete RPMI media (RPMI 1640 medium supplemented with 10% heat-inactivated fetal bovine serum, 50 U/ml penicillin, 50 μM streptomycin, 1 mM sodium pyruvate 2 mM L-glutamine, 0.1 mM non-essential amino acids, 50 μM 2-mercaptoethanol and 10 mM HEPES) (ThermoFisher; Waltham, MA). For magnetic separations, cells were maintained in filtered and degassed MACS buffer: PBS (Lonza; Allendale, NJ, USA) supplemented with 0.5% BSA (Sigma-Aldrich, St. Louis, MO), 2 mM EDTA (Sigma-Aldrich). For the isolation of splenic DCs, Liberase Blendzyme II and DNase (2 μg/ml) were purchased from Roche (Indianapolis, IN).

Samples were stained for flow cytometry using FACS buffer: PBS or HBSS supplemented with 2% FBS, 1% HEPES and 10mM Sodium Azide (Sigma-Aldrich). For confocal microscopy, PBS supplemented with 1% BSA was used as the buffer of choice. Antibodies used for flow cytometry and microscopy are: Anti-CD4-BV786 (Clone RM4–5 for all anti-CD4 antibodies), anti-CD4-BV421, anti-CD4-BV605, anti-anti-CD4-AF488, anti-I-A/I-E-BV421 (Clone M5/114.15.2 for all anti-I-A/I-E antibodies), anti-I-A/I-E-BV605, anti-I-A/I-E-PE, anti-CD3-AF700 (Clone 17A2 for all anti-CD3 antibodies), anti-CD3-BV786, anti-CD45.1-PE.Cy7 (Clone A20, Thermofisher), anti-CD45.2-PE (Clone: 104 for all anti-CD45.2 antibodies), anti-CD45.2-PE.Dazzle 594, anti-CD45.2-APC.Cy7, anti-CD45.2-AF700, anti-CD80-PercpCy5.5 (Clone: 16–10A1), anti-CD86-PE.Cy7 (Clone: GL-1), anti-ICOSL-APC (Clone: HK5.3), anti-PD-L1-BV711 (Clone: 10F.9G2), anti-PD-L2-PE (Clone:TY25), anti-LFA-1-AF647 (Clone:10E5), anti-ICAM-1-PE (Clone: YN1/1.7.4, Thermofisher), Streptavidin-BV650, Streptavidin-QDot525 (ThermoFisher), purified anti-CD16/32 (Clone 93). Antibodies were purchased from Biolegend (San Diego, CA) unless otherwise stated. Anti-MCC_{88-103}-I-E^k (D4) and anti-HEL_{46-61}-I-A^k (AW3.18) were used to detect peptide-MHCII complexes [18, 19]. anti-MCC_{88-103}-I-E^k-AF647, anti-MCC_{88-103}-I-E^k-Biotin, anti-MCC_{88-103}-I-E^k-PE, anti-HEL_{46-61}-I-A^k-AF647 conjugations were performed by Columbia Biosciences (Frederick, MD) Human rIL-2 was obtained from Preclinical Repository of the Biological Resources Branch, National Cancer Institute, Frederick, MD. Recombinant mouse TGF-β_1 was purchased from Peprotech (Rocky Hill, NJ). PCC_{88-104}, MCC_{88-103}, HEL_{46-61}, $OVA_{323-339}$, GP_{61-80} peptides were obtained from NIH Research Technologies Branch, NIAID Peptide Core Facility (Twinbrook, MD). Detailed information on the experimental procedures and reagents are included in the Life Sciences Reporting Summary.

iT_{reg} and $T_{activated}$ differentiation and tT_{reg} proliferation

For iT_{reg} and $T_{activated}$ cell differentiation, naive T cells were isolated and 24 well sterile tissue culture plates (Corning, Corning, NY) were coated anti-CD3ε (145–2C11, Biolegend)

and anti-CD28 (37.51, Biolegend) as described [36]. Naive CD4+ T-cells were resuspended in complete RPMI media supplemented with 100 IU/ml recombinant human IL-2 for both iT$_{reg}$ and T$_{activated}$, with additional 5 ng/ml recombinant human TGF-β for iT$_{reg}$ and 10 μg/ml anti-TGF-β (1D11.16.8, BioXcell, West Lebanon, NH) for T$_{activated}$ cultures. 3×10^5 cells were added to the wells at a volume of 1 ml/well. Cells were cultured at 37°C 5% CO_2 for 3 days. Prior to experiments, live T$_{activated}$ and iT$_{reg}$ were FACS sorted based on their Foxp3-GFP expression status.

IL-2/anti–IL-2 mAb (JES6-1-A12, Bioxcell) complexes were prepared and injected as in [37] to expand antigen-specific tT$_{regs}$ in vivo. Antigen-specific T$_{regs}$ were isolated from spleens of the TCR transgenic animals by FACS sorting based on Foxp3 reporter expression. Alternatively, antigen-specific tT$_{regs}$ were expanded in vitro. For in vitro proliferation, T$_{regs}$ were cultured for three days in the presence of plate bound anti-CD3ε (145–2C11; 2 ug/mL), anti-CD28 (37.51; 2 ug/mL) and IL-2 (100 U/mL). On day 3, cells were split 1:2 and cultured with only IL-2. T$_{regs}$ were harvested on day 5 and FACS sorted for Foxp3 reporter.

Co-cultures

For the isolation of dendritic cells, spleens were removed and flushed by complete RPMI containing Liberase and DNase. Spleens were then fragmented and incubated at 37°C for 30 min. After incubation, RBCs were lysed with ACK-lysing buffer. DCs were isolated using CD11c Microbeads (Miltenyi Biotec) and autoMACS (Miltenyi Biotec) according to manufacturer's protocol.

DCs were pulsed with peptide in complete RPMI and incubated at 37°C for 30 minutes to 3 h (MCC: 30 minutes, HEL: 3 h, OVA: 30 minutes, SMARTA: 30 minutes). They were then washed three times to remove unbound peptide and seeded into flat bottom 96 well plates (Corning) at a density of 5×10^4–10^5 cells/well. iT$_{reg}$ and control T cells were labeled with e450, e670 (eBioscience, San Diego, CA) according to manufacturer's protocol, added at 1:1 ratio with DCs and incubated for 3–18 h for detecting peptide-MHCII acquisition in vitro.

Adoptive transfer

Animals were anesthetized using 1.5 % Isofluorane USP (Baxter, Deerfield, IL) in anesthesia chamber. DCs were resuspended in sterile PBS and injected s.c. into footpads 50 μl/foot. iT$_{reg}$ and control cell types were labeled with e450 or e670 (eBioscience) according to manufacturer's guidelines and injected i.v. in 100 μl PBS per mouse via retro-orbital sinus.

Confocal microscopy

Glass-bottom 14 mm microwell dishes (MatTek, Ashland, MA) were coated with 10 μg/ml Fibronectin (Sigma Aldrich) in PBS at room temperature for one hour and washed twice with complete RPMI. Fresh isolated DCs were seeded in complete RPMI containing 2–5 μM peptide and incubated at 37°C for 1 hour. After washing three times with complete RPMI, iT$_{regs}$ and/or the effector T cells were added. Dishes were further incubated at 37°C for two h. For live imaging, fluorochrome conjugated anti-CD4 was directly added into the culture medium for the last 30 minutes of the culture at 5 μg/ml final concentration. For static

imaging, cultures were fixed with Cytofix/Cytoperm solution (BD Biosciences, San Jose, CA) on ice for 10 minutes, followed by blocking the non-specific interactions using Mouse Serum (Jackson Immunoresearch, West Grove, PA, USA), Fc block in Perm/Wash solution (BD Biosciences) at room temperature for 30 minutes. For staining, cells were incubated with fluorochrome conjugates of anti-I-A/I-E, anti-CD4 and anti-MCC$_{88-103}$-I-E^k antibodies in Perm/Wash solution for 1–2 h at 4°C in dark. After a total of 6 washes using Perm/Wash (X3) and PBS-1%BSA (X3), cells were imaged.

Confocal imaging was performed using a Leica SP-8 inverted microscope equipped with full range of visible lasers, two hybrid detectors (HyDs), 3 photomultiplier detectors (PMTs), and a motorized stage (Leica Microsystems, Buffalo Grove, IL). Immunostained cells were imaged using 63× objective (Leica Microsystems). Microscope configuration was set up for three-dimensional analysis (x,y,z) of cellular layer. The following lasers were used: diode laser for 405 nm excitation; Argon laser for 488 and 514 nm excitation, DPSS laser for 561; and HeNe lasers for 594 and 633 nm excitation wavelengths. All lasers were tuned to minimal power (between 0.3–2%) to prevent photobleaching. Z stack of images of 10–12 μm were collected. Mosaic images of large cell culture areas (1 mm^2) were generated by acquiring multiple Z stacks using Tile scan mode, and assembled into tiled images using LAS X. Images were processed using Imaris (Bitplane, Zurich, Switzerland) software.

Intravital two-photon laser scanning microscopy (TP-LSM) of mouse popliteal lymph node.

TP-LSM setup included Leica SP8 inverted confocal microscope (Leica Microsystems) with dual MP lasers: Mai Tai and InSight DS (Spectra Physics, Santa Clara, CA), and 37° C incubation chamber (NIH Division of Scientific Equipment and Instrumentation Services). Additionally, the microscope was equipped with L 25.0 water-immersion objective, 0.95 NA (Leica Microsystems). Animals were anesthetized using 1.5 % Isofluorane USP, administered via nose cone mask. The surgery was performed on an anaesthetized mouse to expose popliteal lymph node (LN), the mouse was placed on the cover-glass bottom stage, and the LN was kept moisturized with warm PBS and complementarily heated with the infra-red blanket (Braintree Scientific, Braintree MA) over the course of imaging. After imaging, animals were euthanized by cervical dislocation while still under anesthesia. Mai Tai was tuned to 890 nm to excite e450 and YFP; InSight DS was tuned to 1150 nm to excite dsRed and e670. For time-lapse imaging, Z stack consisting of 10–12 single planes (5 μm each over a total tissue depth of 50–60 μm) was acquired every 15 seconds for a total observation time between 1 to 4 h. Post-acquisition image processing was performed using Leica Application Suite (Leica Microsystems), Imaris (Bitplane), and Huygens (Scientific Volume Imaging) software. Cell migration parameters were evaluated using Imaris and GraphPad Prism (GraphPad Software, Inc., La Jolla, CA).

Confocal microscopy of live LN sections.

Confocal imaging of live tissue sections *ex vivo* was developed as a technique for visualizing tissue architecture and cell segregation in the LNs at close to physiological conditions. Mice were euthanized using CO$_2$ chamber (Braintree Scientific), and the LNs were harvested and kept on ice, in 1% BSA in PBS. The LNs were trimmed from residual connective tissue and cords under Leica MZ6 modular stereomicroscope (Leica

Microsystems) using surgical tweezers (Miltex). Preheated 2% agarose (Lonza) in DMEM was chilled to 38°C and immediately poured over the LNs plated in a Petri dish kept on ice. Upon agarose gel polymerization, complete lymphocyte medium was added to the Petri dishes. Agarose gel was cut into cubes each containing one LN, and sliced into 200 μm sections using Leica VT1000 S Vibrating Blade Microtome (Leica Microsystems) at speed 5, in ice-cold PBS. Tissue sections were cultured in complete lymphocyte medium in humidified incubator at 37° C for 2 h and washed with warm medium prior to imaging. Sections were held down with tissue anchors (Warner Instruments) in 14 mm microwell dishes (MatTek), and imaged using Leica SP8 inverted 5 channel confocal microscope equipped with Environmental Chamber (NIH Division of Scientific Equipment and Instrumentation Services) and a motorized stage. Microscope configuration was set up for four-dimensional analysis (x,y,z,t) of cell segregation and migration within tissue sections. Diode laser for 405 nm excitation; Argon laser for 488 and 514 nm excitation, DPSS laser for 561; and HeNe lasers for 594 and 633 nm excitation wavelengths were tuned to minimal power (between 0.3–2%). Z stack of images (10–25 μm). Mosaic images of whole LNs were generated by acquiring multiple Z stacks using motorized stage to cover the whole LN area and assembled into a tiled image using LAS X (Leica Microsystems) software. For time-lapse analysis of cell migration, tiled Z-stacks were collected over time (1 to 4 h). Post-acquisition mages were processed using Imaris (Bitplane) software.

Scanning and Transmission Electron Microscopy

For scanning electron microscopy, samples were processed and imaged essentially as described previously [38]. Briefly, cells were allowed to settle onto Fibronectin (10 μg/ml)-coated silicon chips for 3 h at 37° C, then fixed by replacing buffer with Karnovsky's fixative (Electron Microscopy Sciences, Hatfield, PA). The samples were post-fixed in 1% OsO4 in 0.1M sodium phosphate pH 7.2 using two cycles of 170 W microwave irradiation with power on for 2 min, off for 2 min, and on for 2 min in a BioWave™ model processor (Ted Pella, Inc, Redding, CA). Following two 1 min water washes at 170 W, the samples were dehydrated in 70%, 100%, and 100% ethanol for 1 min each at 250 W, critical point dried through CO_2, and lightly sputtered with iridium. Digital images were captured at 2 kV using a model SU-8000 scanning electron microscope (Hitachi High Technologies, America, Dallas, TX).

For immune transmission electron microscopy, Fibronectin coated cover slips with cell cultures were fixed and processed with modifications to procedures described previously [39, 40]. Samples were pre-fixed in 0.075 M sodium phosphate buffer pH 7.4 containing 0.01M sodium metaperiodate, 0.075M lysine, 2% paraformaldehyde, and 0.25% glutaraldehyde, and held overnight on ice. Subsequent steps were performed at room temperature. Following two 5 min rinses in PBS pH 7.4, cells were permeabilized for 5 min with freshly prepared PBS containing 0.01% saponin (SigmaAldrich). The samples were then probed for 1 hour with the same mixture containing a 1:100 dilution biotinylated anti-MCC_{88-103}-I-E^k (D4). After two washes with PBS, samples were labeled for 1 hr with a 1:50 dilution of Streptavidin conjugated to 525 nm quantum dots in PBS. Following three rinses for 5 min each in PBS, samples were treated for 1 hour with fixative containing 1.5% glutaraldehyde and 5% sucrose in 0.1M sodium phosphate pH 7.4. Further processing steps using

microwave irradiation were conducted as described previously, except that Araldite resin (SPI Inc., West Chester, PA) was used for embedment [41]. Samples were examined and photographed at 80 kV using a model H7500 transmission electron microscope (Hitachi High Technologies), equipped with a model HR-100 CCD camera (Advanced Microscopy Techniques, Woburn, MA)

Trogocytosis assay

DCs were labeled with 4 μM lipophilic membrane dye PKH-26 (Sigma Aldrich) as described in [42], loaded with 3 μM peptide and co-cultured with T cells for 18 h. Cell conjugates were dissociated washing the cells with MACS buffer containing 2 mM EDTA and cell suspensions were prepared for flow cytometry.

Flow Cytometry

Cells were washed with MACS buffer, followed by FACS buffer and stained with fluorochrome-conjugated antibodies at 4 ˚C for 30 min in dark. Cells were barcoded as in [43] wherever indicated. Data acquisition was performed using BD Fortessa and BD LSR-II cytometers (BD Biosciences). Data were analyzed in FlowJo software.

Image Analysis

Imaris (Bitplane) software was used to analyze confocal microscopy and intravital two photon microscopy data. SEM and TEM data were analyzed by Image J (NIH). Normalized velocity in Figure 3 was calculated as: (Mean track speed of naive OT-II-DsRed/ Average for the mean track speeds of polyclonal CD4$^+$). In Figure 6b, the YFP (CD11c) signal was used to reconstruct the 3D structure of the DC as a surface object. DCs were then removed as 3D objects from the CD45.1 (AF647, red) channel. The resulting masked CD45.1 (Red) channel (with DC portion removed) was utilized to reconstruct CD45.1$^+$ cells and MHCII (Blue) intensities of these cells were quantified.

Statistical Analysis

Statistical significance analyses were performed using GraphPad Prism, version 7.0d. Statistical tests and P values are indicated in the figures and figure legends. Briefly, while comparing two continuous interval variables with normal distribution, two-sided students' t-test and two-sided Welch's t-test were used. For comparing three or more continuous interval variables, either one-way or two-way ANOVA is used depending on the experimental set up. Non-parametric tests such as Kolmogorov-Smirnov, and Kruskal-Wallis are selected for determining the statistical significance to compare three or more distribution free discrete variables as appropriate and mentioned in the figure legends.

Supplementary Material

Refer to Web version on PubMed Central for supplementary material.

## ACKNOWLEDGEMENTS

REFERENCES

1. Samy ET, Parker LA, Sharp CP & Tung KS Continuous control of autoimmune disease by antigen-dependent polyclonal CD4+CD25+ regulatory T cells in the regional lymph node. J Exp Med 202, 771–781 (2005). [PubMed: 16172257]

2. Andersson J et al. CD4+ FoxP3+ regulatory T cells confer infectious tolerance in a TGF-beta-dependent manner. J Exp Med 205, 1975–1981 (2008). [PubMed: 18710931]

3. Borsellino G et al. Expression of ectonucleotidase CD39 by Foxp3+ Treg cells: hydrolysis of extracellular ATP and immune suppression. Blood 110, 1225–1232 (2007). [PubMed: 17449799]

4. Collison LW et al. The inhibitory cytokine IL-35 contributes to regulatory T-cell function. Nature 450, 566–569 (2007). [PubMed: 18033300]

5. Shevach EM Mechanisms of foxp3+ T regulatory cell-mediated suppression. Immunity 30, 636–645 (2009). [PubMed: 19464986]

6. Pandiyan P, Zheng L, Ishihara S, Reed J & Lenardo MJ CD4+CD25+Foxp3+ regulatory T cells induce cytokine deprivation-mediated apoptosis of effector CD4+ T cells. Nat Immunol 8, 1353–1362 (2007). [PubMed: 17982458]

7. Wing K et al. CTLA-4 control over Foxp3+ regulatory T cell function. Science 322, 271–275 (2008). [PubMed: 18845758]

8. Qureshi OS et al. Trans-endocytosis of CD80 and CD86: a molecular basis for the cell-extrinsic function of CTLA-4. Science 332, 600–603 (2011). [PubMed: 21474713]

9. Cao X et al. Granzyme B and perforin are important for regulatory T cell-mediated suppression of tumor clearance. Immunity 27, 635–646 (2007). [PubMed: 17919943]

10. Thornton AM & Shevach EM Suppressor effector function of CD4+CD25+ immunoregulatory T cells is antigen nonspecific. J Immunol 164, 183–190 (2000). [PubMed: 10605010]

11. Thornton AM & Shevach EM CD4+CD25+ immunoregulatory T cells suppress polyclonal T cell activation in vitro by inhibiting interleukin 2 production. J Exp Med 188, 287–296 (1998). [PubMed: 9670041]

12. Tang Q et al. Visualizing regulatory T cell control of autoimmune responses in nonobese diabetic mice. Nat Immunol 7, 83–92 (2006). [PubMed: 16311599]

13. Tadokoro CE et al. Regulatory T cells inhibit stable contacts between CD4+ T cells and dendritic cells in vivo. J Exp Med 203, 505–511 (2006). [PubMed: 16533880]

14. Rossy J, Williamson DJ, Benzing C & Gaus K The integration of signaling and the spatial organization of the T cell synapse. Front Immunol 3, 352 (2012). [PubMed: 23189081]

15. Hashimoto-Tane A & Saito T Dynamic Regulation of TCR-Microclusters and the Microsynapse for T Cell Activation. Front Immunol 7, 255 (2016). [PubMed: 27446085]

16. Doh J & Krummel MF Immunological synapses within context: patterns of cell-cell communication and their application in T-T interactions. Curr Top Microbiol Immunol 340, 25–50 (2010). [PubMed: 19960307]

17. Yokosuka T et al. Spatiotemporal regulation of T cell costimulation by TCR-CD28 microclusters and protein kinase C theta translocation. Immunity 29, 589–601 (2008). [PubMed: 18848472]

18. Irvine DJ, Purbhoo MA, Krogsgaard M & Davis MM Direct observation of ligand recognition by T cells. Nature 419, 845–849 (2002). [PubMed: 12397360]

19. Dadaglio G, Nelson CA, Deck MB, Petzold SJ & Unanue ER Characterization and quantitation of peptide-MHC complexes produced from hen egg lysozyme using a monoclonal antibody. Immunity 6, 727–738 (1997). [PubMed: 9208845]

20. Yan J, Liu B, Shi Y & Qi H Class II MHC-independent suppressive adhesion of dendritic cells by regulatory T cells in vivo. J Exp Med 214, 319–326 (2017). [PubMed: 28082359]

21. Chen J et al. Strong adhesion by regulatory T cells induces dendritic cell cytoskeletal polarization and contact-dependent lethargy. J Exp Med 214, 327–338 (2017). [PubMed: 28082358]

Author Manuscript Author Manuscript Author Manuscript Author Manuscript

22. Ahmed KA, Munegowda MA, Xie Y & Xiang J Intercellular trogocytosis plays an important role in modulation of immune responses. Cell Mol Immunol 5, 261–269 (2008). [PubMed: 18761813]

23. Patel DM, Arnold PY, White GA, Nardella JP & Mannie MD Class II MHC/peptide complexes are released from APC and are acquired by T cell responders during specific antigen recognition. J Immunol 163, 5201–5210 (1999). [PubMed: 10553040]

24. Hwang I et al. T cells can use either T cell receptor or CD28 receptors to absorb and internalize cell surface molecules derived from antigen-presenting cells. J Exp Med 191, 1137–1148 (2000). [PubMed: 10748232]

25. Zhou G, Ding ZC, Fu J & Levitsky HI Presentation of acquired peptide-MHC class II ligands by CD4+ regulatory T cells or helper cells differentially regulates antigen-specific CD4+ T cell response. J Immunol 186, 2148–2155 (2011). [PubMed: 21242518]

26. Zanin-Zhorov A et al. Protein kinase C-theta mediates negative feedback on regulatory T cell function. Science 328, 372–376 (2010). [PubMed: 20339032]

27. Chatila TA & De Palma R A simple twist of phosphate: Immunological synapse formation and T cell receptor signaling outcome in regulatory T cells. Eur J Immunol 47, 2039–2042 (2017). [PubMed: 29211935]

28. Onishi Y, Fehervari Z, Yamaguchi T & Sakaguchi S Foxp3+ natural regulatory T cells preferentially form aggregates on dendritic cells in vitro and actively inhibit their maturation. Proc Natl Acad Sci U S A 105, 10113–10118 (2008). [PubMed: 18635688]

29. Matheu MP et al. Imaging regulatory T cell dynamics and CTLA4-mediated suppression of T cell priming. Nat Commun 6, 6219 (2015). [PubMed: 25653051]

30. Mittelbrunn M et al. VLA-4 integrin concentrates at the peripheral supramolecular activation complex of the immune synapse and drives T helper 1 responses. Proc Natl Acad Sci U S A 101, 11058–11063 (2004). [PubMed: 15263094]

31. Sarris M, Andersen KG, Randow F, Mayr L & Betz AG Neuropilin-1 expression on regulatory T cells enhances their interactions with dendritic cells during antigen recognition. Immunity 28, 402–413 (2008). [PubMed: 18328743]

32. Levine AG, Arvey A, Jin W & Rudensky AY Continuous requirement for the TCR in regulatory T cell function. Nat Immunol 15, 1070–1078 (2014). [PubMed: 25263123]

33. Vahl JC et al. Continuous T cell receptor signals maintain a functional regulatory T cell pool. Immunity 41, 722–736 (2014). [PubMed: 25464853]

34. Schmidt AM et al. Regulatory T cells require TCR signaling for their suppressive function. J Immunol 194, 4362–4370 (2015). [PubMed: 25821220]

35. Barda-Saad M et al. Cooperative interactions at the SLP-76 complex are critical for actin polymerization. EMBO J 29, 2315–2328 (2010). [PubMed: 20562827]

36. Akkaya B et al. Ex-vivo iTreg differentiation revisited: Convenient alternatives to existing strategies. J Immunol Methods 441, 67–71 (2017). [PubMed: 27919837]

37. Chen Q, Kim YC, Laurence A, Punkosdy GA & Shevach EM IL-2 controls the stability of Foxp3 expression in TGF-beta-induced Foxp3+ T cells in vivo. J Immunol 186, 6329–6337 (2011). [PubMed: 21525380]

38. Kumar S et al. Zinc-Induced Polymerization of Killer-Cell Ig-like Receptor into Filaments Promotes Its Inhibitory Function at Cytotoxic Immunological Synapses. Mol Cell 62, 21–33 (2016). [PubMed: 27058785]

39. Chaturvedi A, Dorward D & Pierce SK The B cell receptor governs the subcellular location of Toll-like receptor 9 leading to hyperresponses to DNA-containing antigens. Immunity 28, 799–809 (2008). [PubMed: 18513998]

40. Akkaya M et al. Toll-like receptor 9 antagonizes antibody affinity maturation. Nat Immunol 19, 255–266 (2018). [PubMed: 29476183]

41. Offerdahl DK, Dorward DW, Hansen BT & Bloom ME A three-dimensional comparison of tick-borne flavivirus infection in mammalian and tick cell lines. PLoS One 7, e47912 (2012). [PubMed: 23112871]

42. Puaux AL et al. A very rapid and simple assay based on trogocytosis to detect and measure specific T and B cell reactivity by flow cytometry. Eur J Immunol 36, 779–788 (2006). [PubMed: 16482513]

43. Akkaya B et al. A Simple, Versatile Antibody-Based Barcoding Method for Flow Cytometry. J Immunol 197, 2027–2038 (2016). [PubMed: 27439517]

REFERENCES FOR METHODS

46. Akkaya B et al. Ex-vivo iTreg differentiation revisited: Convenient alternatives to existing strategies. J Immunol Methods 441, 67–71 (2017) [PubMed: 27919837]

47. Chen Q, Kim YC, Laurence A, Punkosdy GA & Shevach EM IL-2 controls the stability of Foxp3 expression in TGF-beta-induced Foxp3+ T cells in vivo. J Immunol 186, 6329–6337 (2011). [PubMed: 21525380]

48. Kumar S et al. Zinc-Induced Polymerization of Killer-Cell Ig-like Receptor into Filaments Promotes Its Inhibitory Function at Cytotoxic Immunological Synapses. Mol Cell 62, 21–33 (2016). [PubMed: 27058785]

49. Chaturvedi A, Dorward D & Pierce SK The B cell receptor governs the subcellular location of Toll-like receptor 9 leading to hyperresponses to DNA-containing antigens. Immunity 28, 799–809 (2008). [PubMed: 18513998]

50. Akkaya M et al. Toll-like receptor 9 antagonizes antibody affinity maturation. Nat Immunol 19, 255–266 (2018). [PubMed: 29476183]

51. Offerdahl DK, Dorward DW, Hansen BT & Bloom ME A three-dimensional comparison of tick-borne flavivirus infection in mammalian and tick cell lines. PLoS One 7, e47912 (2012). [PubMed: 23112871]

52. Puaux AL et al. A very rapid and simple assay based on trogocytosis to detect and measure specific T and B cell reactivity by flow cytometry. Eur J Immunol 36, 779–788 (2006). [PubMed: 16482513]

53. Akkaya Bet al. A Simple, Versatile Antibody-Based Barcoding Method for Flow Cytometry. J Immunol 197, 2027–2038 (2016). [PubMed: 27439517]
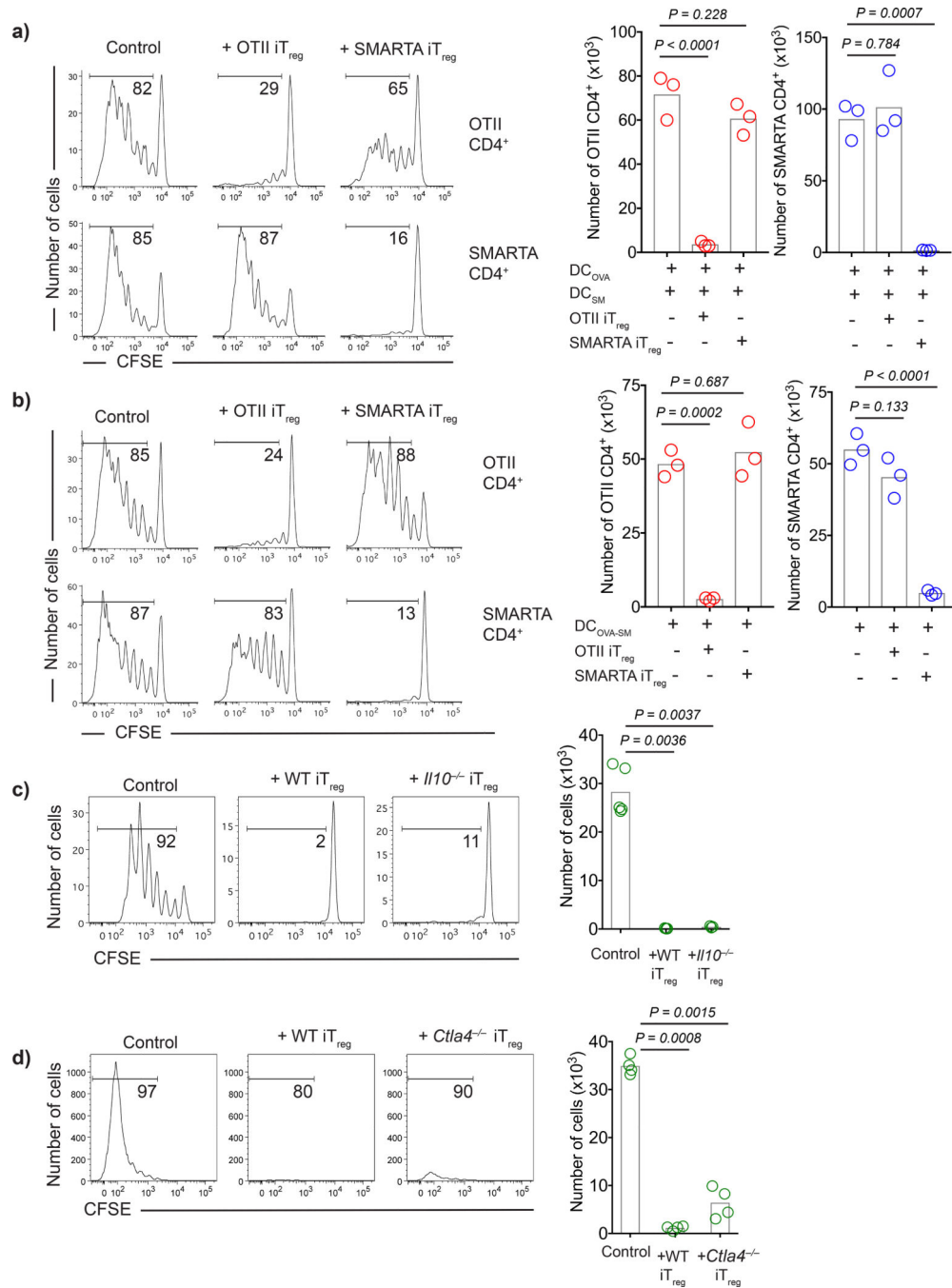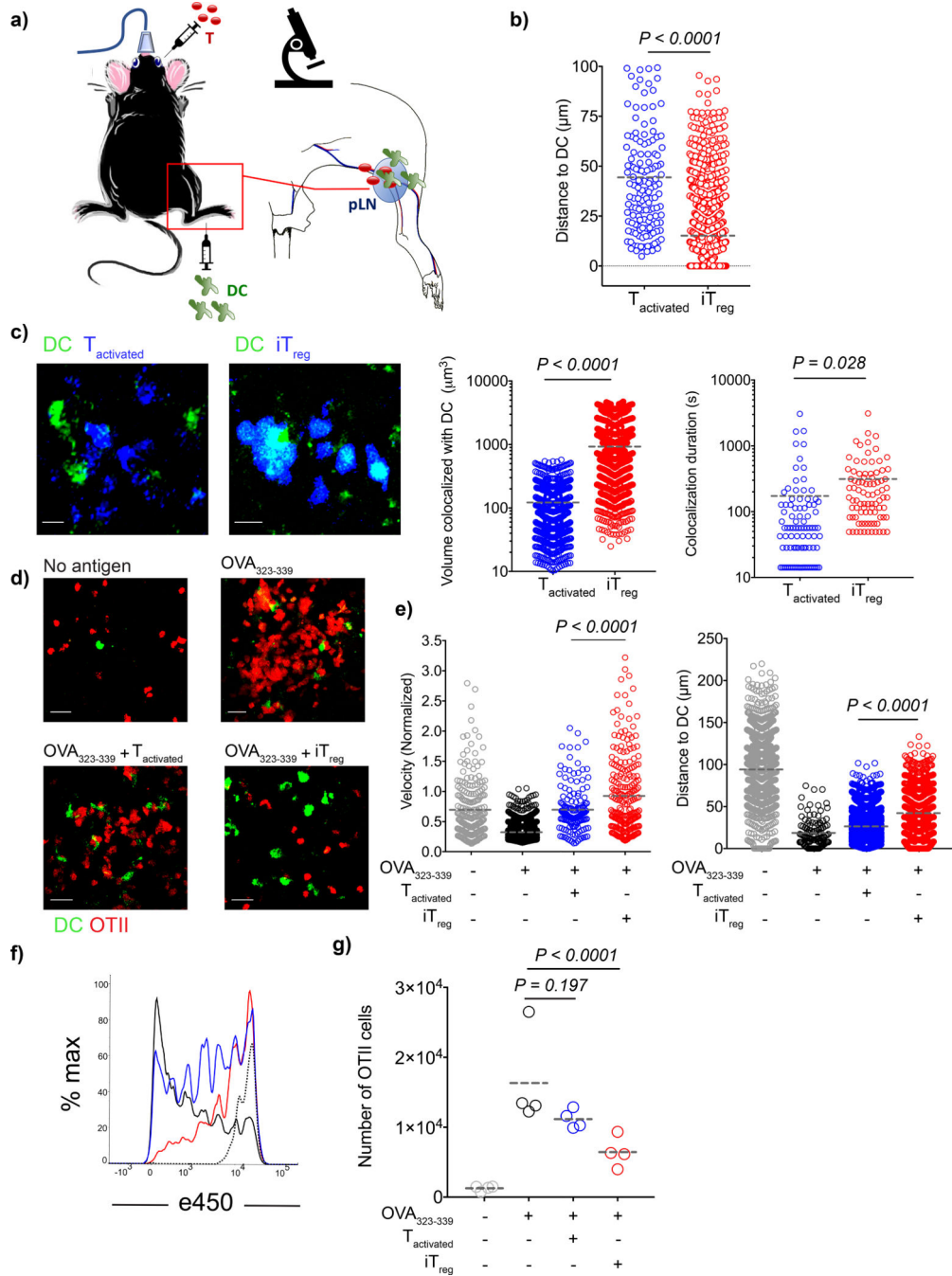
Figure 1:

Antigen-specific iT$_{regs}$ suppress T$_{naive}$ cells with identical antigen specificity regardless of CTLA-4 expression or IL-10 production. **a-b)** C57BL/6 DCs were loaded with 3 μM OVA$_{323-339}$ (DC$_{OVA}$), LCMV GP$_{61-80}$ (DC$_{GP}$) or both peptides (DC$_{OVA-GP}$). CFSE labeled naive OT-II (1×10^6) and SMARTA (1×10^6) cells were transferred i.v. into CD45.1 mice with DCs (5×10^5) and iT$_{regs}$ (2×10^6). Histograms demonstrate day 3 post-transfer proliferation status of Thy1.1$^-$ OT-II and Thy1.1$^+$ SMARTA cells upon co-transfer with 1:1 mixture of DC$_{OVA}$ and DC$_{GP}$ **(a)** or DC$_{OVA-GP}$ **(b)**. Graphs show the number of CFSE^{low} proliferating

cells. **c-d)** B10.A DCs were pulsed with 3 μM PCC_{88-104}. $CD45.1^+$ CFSE labeled 5CC7 T_{naive} (1×10^6) were transferred i.v. into B10.A mice together with DCs (5×10^5) and WT, $Il10^{-/-}$ or $Ctla4^{-/-}$ 5CC7 iT_{regs} (2×10^6). Histograms demonstrate the day 3 post-transfer proliferation states, graphs show the number of $CFSE^{low}$ 5CC7 T cells. Bars indicate the means of n=3 mice, data are representative of two (c,d) or three (a,b) independent experiments. *P* values were calculated using one-way ANOVA with Dunnett's multiple comparison test.
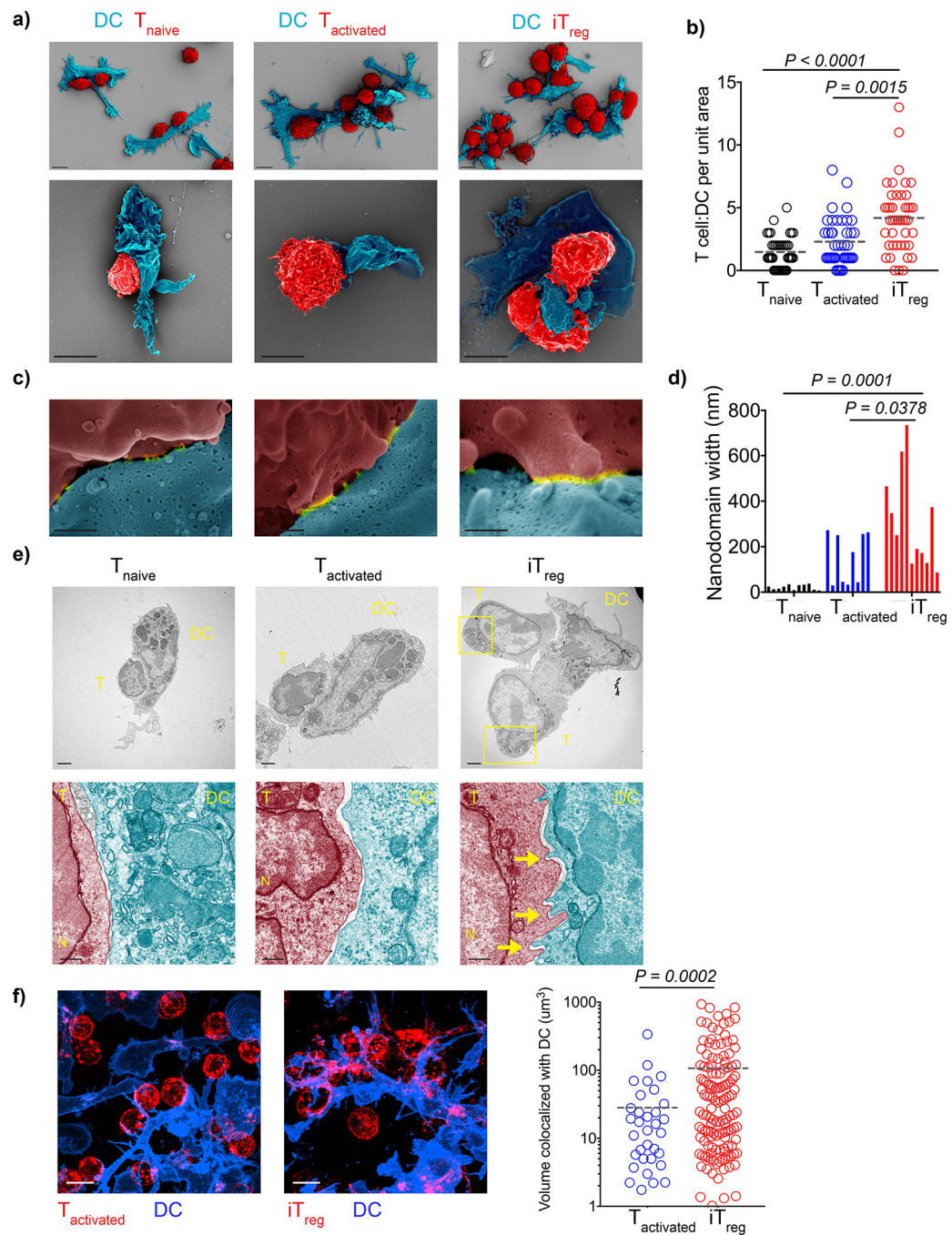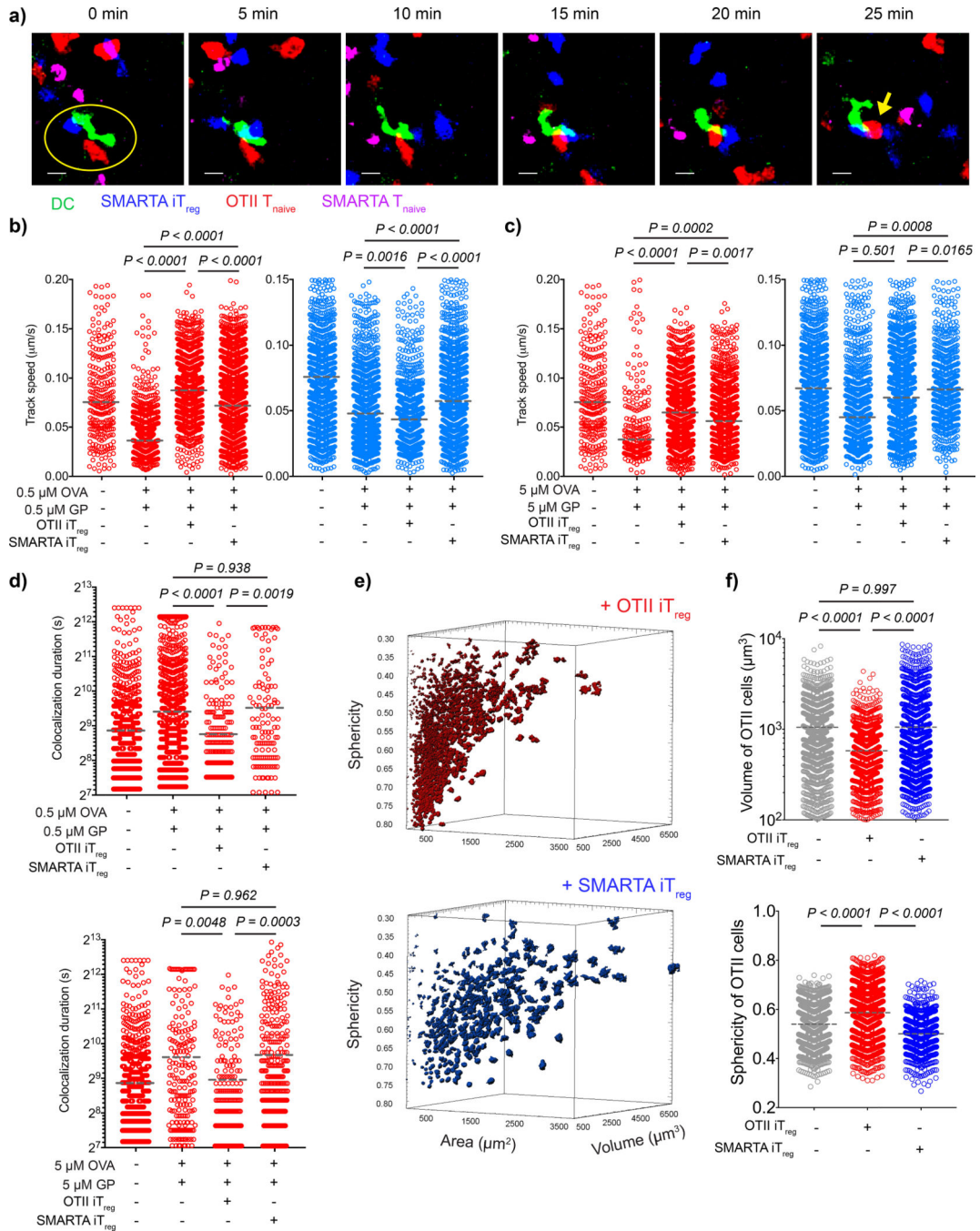
Figure 2:

Antigen-specific iT$_{regs}$ have unique binding morphology and stoichiometry. **a-d)** OVA$_{323-339}$ pulsed splenic DCs (4×10^4) were co-cultured 1:1 with OT-II T$_{naive}$, OT-II T$_{activated}$ or OT-II iT$_{regs}$ for 3 h and visualized by SEM. **a)** Representative images of T-DC clusters (Scale bar: 5 μm). **b)** Images were collected from a total of 40 DCs, graph shows the number of T cells bound per DC. Lines mark the means of n=40 DCs obtained from n=2 biological replicates per experiment. Data are representative of two independent experiments. **c)** SEM images of the DC-T cell binding sites which reveal membrane fusion

domains (nanodomains) (Scale bar: 300 nm). **d)** n=2 biological replicates were screened to collect images of 9–11 fusion sites per group. Bars demonstrate individual measurements pooled from the replicates, data represent three independent experiments. **e)** OVA$_{323-339}$ pulsed DCs (2×10^5) were co-cultured 1:1 with OT-II T$_{naive}$, OT-II T$_{activated}$ or OT-II iT$_{reg}$ on for 3 h and imaged with TEM. Yellow rectangles and arrows mark the uropods and filopodia respectively. Scale bars for images are upper: 2 μm, lower: 500 nm. Images are representative of three independent experiments with similar results. **f)** OVA$_{323-339}$ pulsed DCs (2×10^5) were co-cultured 1:1 with OT-II T$_{activated}$ or OT-II iT$_{reg}$ for 3h and imaged for real time interactions (CD4: Red, CD11c: Blue). Graph shows the 3D volume of T-DC contact site that was derived from time dependent colocalization analysis. Lines mark the mean of individual data points pooled from n=2 biological replicates. Data are representative of five independent experiments with similar results. *P* values were calculated using Kruskal-Wallis (b), one-way ANOVA (d), two-sided Welch's t-test (f).

Figure 3:

Antigen specific iT_{regs}, but not $T_{activated}$, form compact clusters around DCs and inhibit T_{naive} cell priming. **a-e)** CD11c-YFP DCs (2×10^6) were loaded with 5 μM $OVA_{323-339}$ and adoptively transferred into C57BL/6 mice via the footpad. Popliteal lymph nodes of the recipient mice were imaged with intravital two photon microscopy at 18–20 h post-transfer. **a)** Schematic representation of the experiment. **b-c)** e450-labeled OT-II $T_{activated}$ or iT_{regs} (4×10^6) were adoptively transferred. **b)** Graph shows distance of T cells to the closest DC. Lines mark the means of the cells from one recipient, data are representative of n=4

independent experiments with similar results. **c)** Images demonstrate the in vivo interaction of $T_{activated}$ and iT_{regs} with DCs 18–20 h post-transfer. Graphs are derived from the time dependent colocalization analysis for the dynamic T-DC contact at 20–22 h post-transfer. Lines mark the means of the cells from one recipient, data are representative of n=4 independent experiments with similar results. **d-e)** C57BL/6 mice received naive OT-II-DsRed cells (5×10^6), naive e670-labeled polyclonal $CD4^+$ T cells (10^7) with or without e450-labeled OT-II $T_{activated}$ or iT_{reg} (10^7). **d)** Images demonstrate the position and clustering of naive OT-II-DsRed cells around DCs. **e)** Tracks of the naive OT-II-DsRed cells and polyclonal $CD4^+$ T cells were analyzed and calculations were performed as described in methods. Lines mark the means of the cells from one recipient, data are representative of n=3 independent experiments with similar results. **f-g)** DCs were loaded with 5 μM $OVA_{323–339}$ ex-vivo. DCs (3×10^5) were adoptively transferred into C57BL/6 mice via the footpad. The mice then received naive e450 labeled $CD45.1^+$ OT-II cells (10^6) with or without OT-II $T_{activated}$ or iT_{regs} (4×10^6) i.v. **f)** Histograms demonstrate the day 3 post-transfer proliferation status of $CD45.1^+$ OT-II cells when transferred alone (Black), co-transferred with OT-II $T_{activated}$ (Blue), or co-transferred with OT-II iT_{regs} (Red). Dotted histogram shows the proliferation status of $CD45.1^+$ OT-II cells in the mice which received unpulsed DCs. **g)** Number of $CD45.1^+$ OT-II cells in the lymph nodes. Lines mark the mean of n=4 mice, data are representative of three independent experiments. *P* values were calculated using two-sided student's t-test (b,c), Kolmogorov-Smirnov (velocity, e), one-way ANOVA with Tukey's test (distance, e) and with Dunnett's test (g).
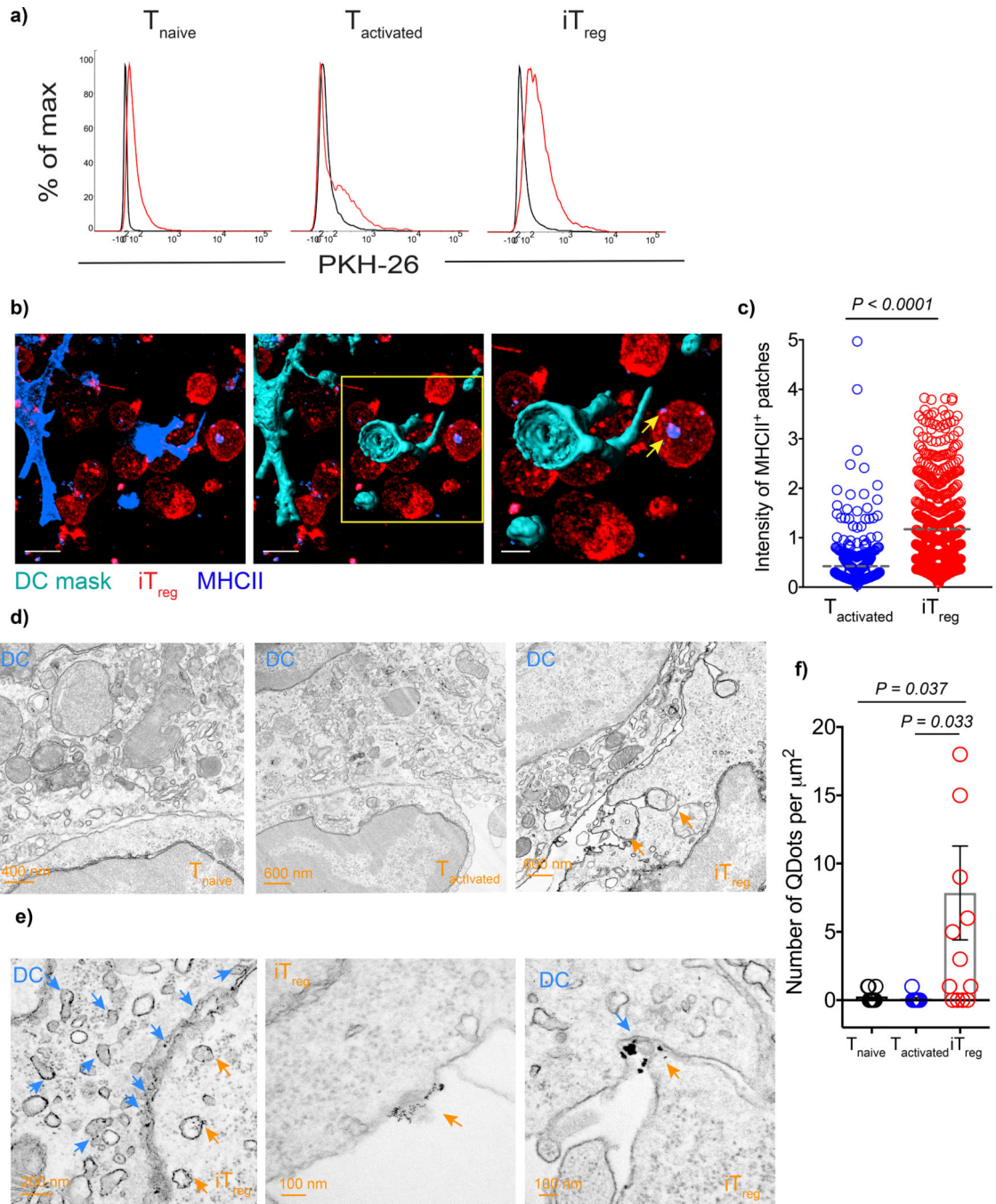
Figure 4:

Antigen-specific iT$_{regs}$ inhibit the stable contact of T cells and DCs in TCR restricted manner. **a-d)** Splenic DCs from CD11c-YFP animals were double pulsed with OVA$_{323-339}$ and LCMV GP$_{61-80}$ at either 0.5 μM or 5 μM ex-vivo. DCs (2×10^6) were adoptively transferred into C57BL/6 mice via the footpad. The mice then received naive OT-II-DsRed (1.2×10^6), naive e670-labeled SMARTA T cells (1.2×10^6) and e450-labeled OT-II or SMARTA iT$_{regs}$ (4.8×10^6) i.v. Live popliteal lymph node sections were imaged 18 h post-transfer. **a)** Time series demonstrate the movement and interactions of SMARTA iT$_{regs}$, OT-

II-DsRed T_{naive}, SMARTA T_{naive} with 5 min intervals. Yellow circle represents the contact with DC. Yellow arrow shows the OT-II T_{naive} that had sustained interaction with the DC (Scale bar: 20 μm). **b-d)** Graphs show the average track speed (b,c) and colocalization duration (d) of OT-II and SMARTA, Lines mark the means of the cells tracked in one recipient, data are representative of n=3 independent experiments with similar results. **e-f)** DCs (2×10^6) double pulsed with 5 μM $OVA_{323-339}$ and GP_{61-80} were adoptively transferred via footpad. Naive OT-II-DsRed T cells (7×10^6) were transferred i.v. together with either e450-labeled OT-II iT_{reg} or SMARTA iT_{reg} (1.4×10^7). Popliteal lymph node sections were imaged 18–20 h post-transfer. Representative demonstration (e) and graphs (f) of 3D surface area, volume and sphericity of OT-II T_{naives}. Lines mark the means of the cells from one recipient, data are representative of n=3 independent experiments with similar results. *P* values were calculated using one-way ANOVA with Tukey's correction (b,c,d,f-volume) and Kruskal-Wallis (f-sphericity).
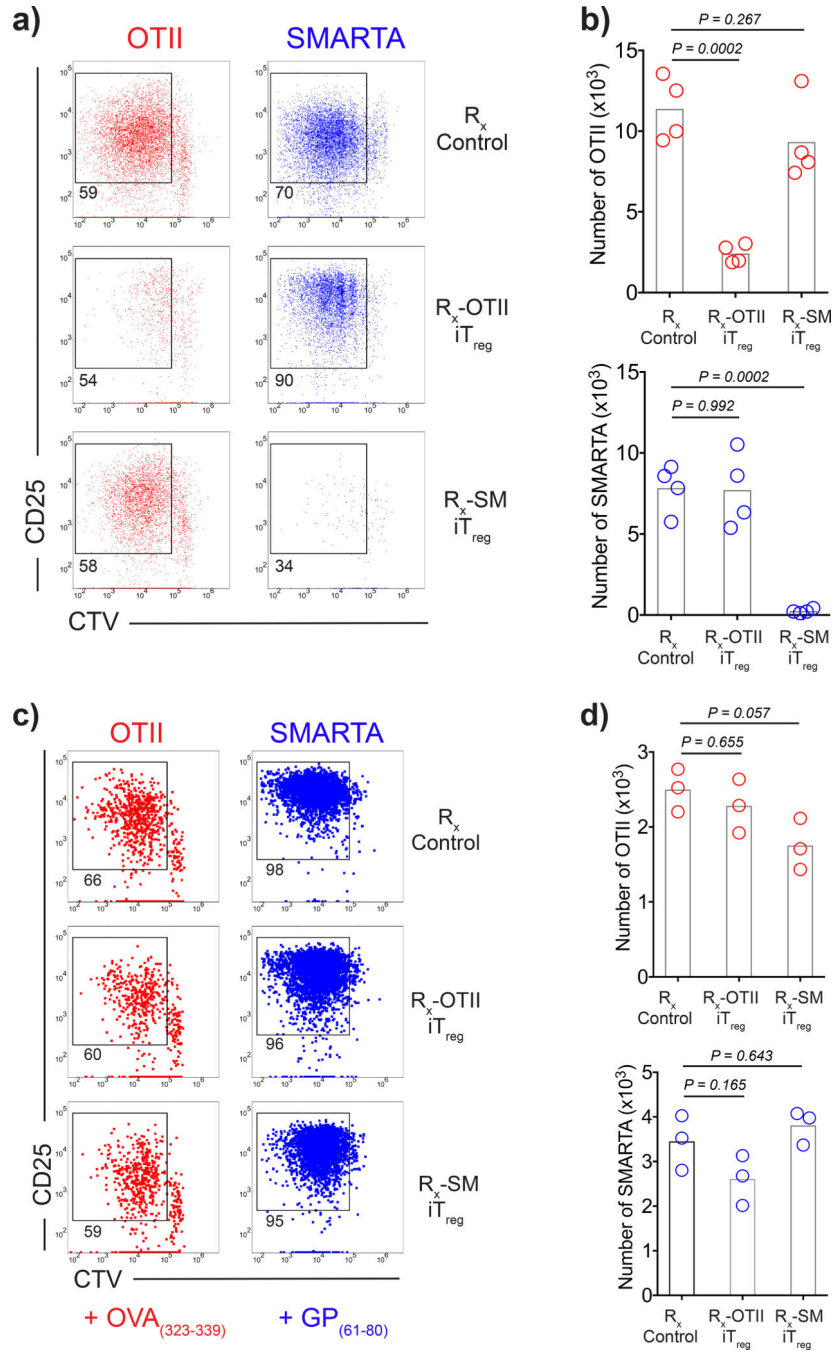
Figure 5:

Antigen-specific iT_{regs} selectively inhibit presentation of cognate antigen. **a-b)** DCs (4×10^6) were double-pulsed with 3 μM $OVA_{323-339}$ and 3 μM LCMV GP_{61-80} and cultured with CFSE-labeled OT-II iT_{regs} (1.5×10^6) (R_x-OT-II iT_{reg}), SMARTA iT_{regs} (1.5×10^6) (R_x-SM iT_{reg}) or alone (R_x-Control) for 18 h; live $CFSE^- CD3\varepsilon^-$ DCs were isolated by FACS sorting. **a-b)** Sorted DCs (5×10^3) were co-cultured with 1:1 mixture of CTV (Cell Tracker Violet) labeled $CD45.1^+$ OT-II (5×10^4) and SMARTA (5×10^4) T_{naives} for 3 days. **a)** Flow cytometry plots demonstrate the proliferation status and CD25 expression of T_{naive}. **b)** Graphs show

numbers of CFSE^{low} T cells. Bars indicate the means of n=3 biological replicates, data are representative of two independent experiments. **c-d)** Sorted DCs (5×10^3) were pulsed with either OVA$_{323-339}$ or LCMV GP$_{61-80}$ and cultured with CTV labeled CD45.1$^+$ OT-II or SMARTA T$_{naives}$ (5×10^4) for 3 days. **c)** Flow cytometry plots demonstrate the proliferation status and CD25 expression of T$_{naive}$. **d)** Graphs show numbers of CFSE^{low} T cells. Bars indicate the means of n=3 biological replicates, data are representative of two independent experiments. *P* values were calculated using one-way ANOVA with Dunnett's post-test.

Figure 6:

Antigen-specific iT$_{regs}$ have greater trogocytic capacity. **a)** DCs were labeled with PKH-26, loaded with 3 μM MCC$_{(88–103)}$ and co-cultured 1:1 with 5CC7 T$_{naive}$, T$_{activated}$ or iT$_{regs}$ for 18 h. Histograms show the intensity of PKH-26 on T cells upon co-culture, black: T cells co-cultured with unpulsed DC, red: T cells co-cultured with antigen pulsed DC. Data are representative of three independent experiments that were performed in triplicates. **b-c)** CD11c-YFP DCs were loaded with 3 μM OVA$_{(323–339)}$ peptide and co-cultured with OT-II T$_{activated}$ (CD45.1$^+$) or OT-II iT$_{regs}$ (CD45.1$^+$) for 3 h. **b)** Representative images showing 3D

surfaces created to mask the DCs based on CD11c-YFP intensity. Yellow arrows point to the MHCII$^+$ patches on iT$_{regs}$. **c)** Graph shows MHCII intensity of OT-II T$_{activated}$ and OT-II iT$_{regs}$. Lines mark the mean of individual data points pooled from n=2 biological replicates. Data are representative of three independent experiments with similar results. **d-f)** DCs were loaded with 3 μM MCC$_{(88-103)}$ and co-cultured with 5CC7 T$_{naive}$, T$_{activated}$ or iT$_{regs}$ for 3 h. Sections were stained with biotinylated anti-MCC$_{(88-103)}$-I-E^k antibody (D4) antibody followed by streptavidin conjugated quantum dots. **d)** TEM images demonstrate T$_{naive}$, T$_{activated}$ and iT$_{reg}$ contacts with DC. Orange arrow heads mark the patches of DC membrane captured by iT$_{regs}$. **e)** Higher magnification images of DC-iT$_{reg}$ contact. Orange arrow heads point to the endosomes and membrane parts containing quantum dots. Blue arrow heads show the positive quantum dot staining in the DCs. **f)** Bars indicate the mean amount of quantum dots per μm^2, error bars show the standard error of the mean. Data are pooled from n=3 independent experiments with similar results, each performed with two biological replicates. *P* values were calculated using two-sided student's t-test (c) and one-way ANOVA with Dunnett's post-test (f).
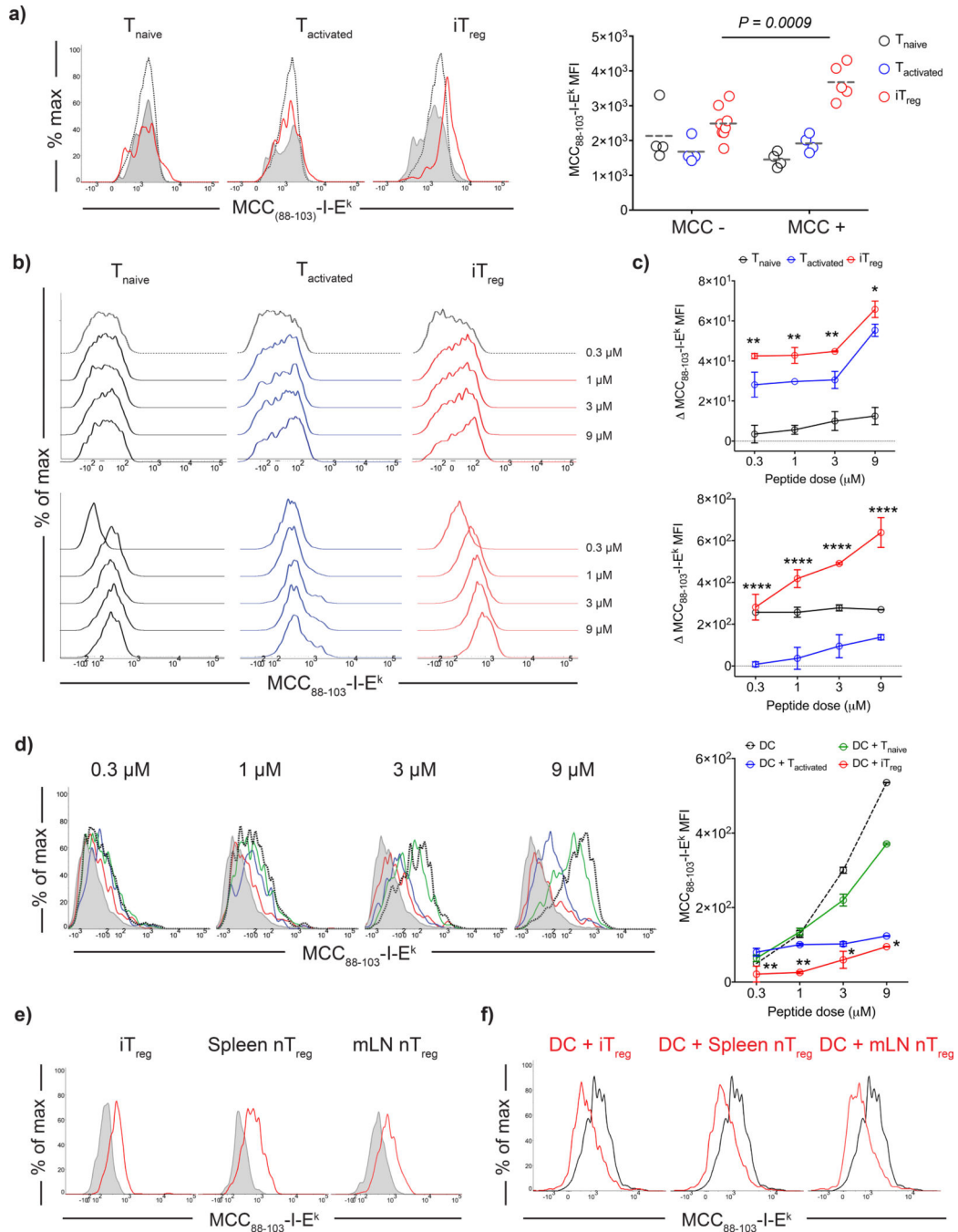
Figure 7:
Antigen-specific T_{reg}s strip cognate pMHCII complexes from DC surface. **a)** DCs were loaded with 3 μM $MCC_{(88–103)}$ (MCC +) or left unpulsed (MCC -) and adoptively transferred into $CD45.1^+B10.A$ mice via footpad, followed by a transfer of e450 labeled 5CC7 T_{naive}, $T_{activated}$ or iT_{regs} (10^6) i.v. Histograms demonstrate day 3 post-transfer $MCC_{(88–103)}$-I-E^k levels of adoptively transferred T cells: Red: co-transferred with antigen pulsed DC. Black dotted: co-transferred with unpulsed DC. Endogenous $CD4^+$ T cells of the recipient mice (Gray tinted) were also plotted as an internal negative control for staining.

Graph shows the $MCC_{(88-103)}$-I-E^k MFIs of adoptively transferred T cells. Lines mark the mean of n=4–8 mice, data are representative of three independent experiments. **b-d)** DCs were loaded with 0.3 – 9 µM $MCC_{(88-103)}$ and co-cultured 1:1 with 5CC7 T_{naive}, $T_{activated}$ or iT_{regs} for 18 h. **b)** Histograms demonstrate the $MCC_{(88-103)}$-I-E^k levels in the T cell gate. Upper row shows the surface levels, lower row shows the intracellular levels detected after blockade of the surface $MCC_{(88-103)}$-I-E^k by unconjugated D4 antibody. **c)** Graphs show the net increase in the $MCC_{(88-103)}$-I-E^k MFI at the surface (top) and intracellular (bottom) compartments of T cells (Δ MFI= MFI $_{(Post\text{- antigen pulsed DC co-culture})}$ - MFI $_{(Post\text{- unpulsed DC co-culture})}$). Symbols and error bars indicate the mean and standard deviation of n=3 biological replicates. Data are representative of five independent experiments. **d)** Histograms demonstrate the $MCC_{(88-103)}$-I-E^k surface levels in the DC gate (Gray tinted: unpulsed DC; black dotted: antigen pulsed DC; antigen pulsed DCs co-cultured with T_{naive}, $T_{activated}$ and iT_{regs} were shown by green, blue and red histograms respectively). Graph shows the MFI for DC surface $MCC_{(88-103)}$-I-E^k. Symbols and error bars indicate the mean and standard deviation of n=3 biological replicates. Data are representative of five independent experiments. **e-f)** 5CC7 iT_{reg}, splenic (Sp) and mesenteric lymph node (mLN) T_{reg} were co-cultured with DCs that were loaded with 3 µM $MCC_{(88-103)}$. **e)** Histograms show the $MCC_{(88-103)}$-I-E^k levels in T_{reg} gate following the co-culture with unpulsed DC (Gray tinted) and antigen pulsed DC (Red). **f)** Histograms show the $MCC_{(88-103)}$-I-E^k levels in DC gate following the co-culture with different antigen specific T_{reg} types. Black histogram shows the antigen pulsed DC cultured alone, red histogram shows the remaining levels $MCC_{(88-103)}$-I-E^k after Treg-DC co-culture. Data are representative of three independent experiments with similar results. Statistical significance was calculated using two-way ANOVA with Sidak's multiple comparison (a) and Dunnet's correction (c,d).
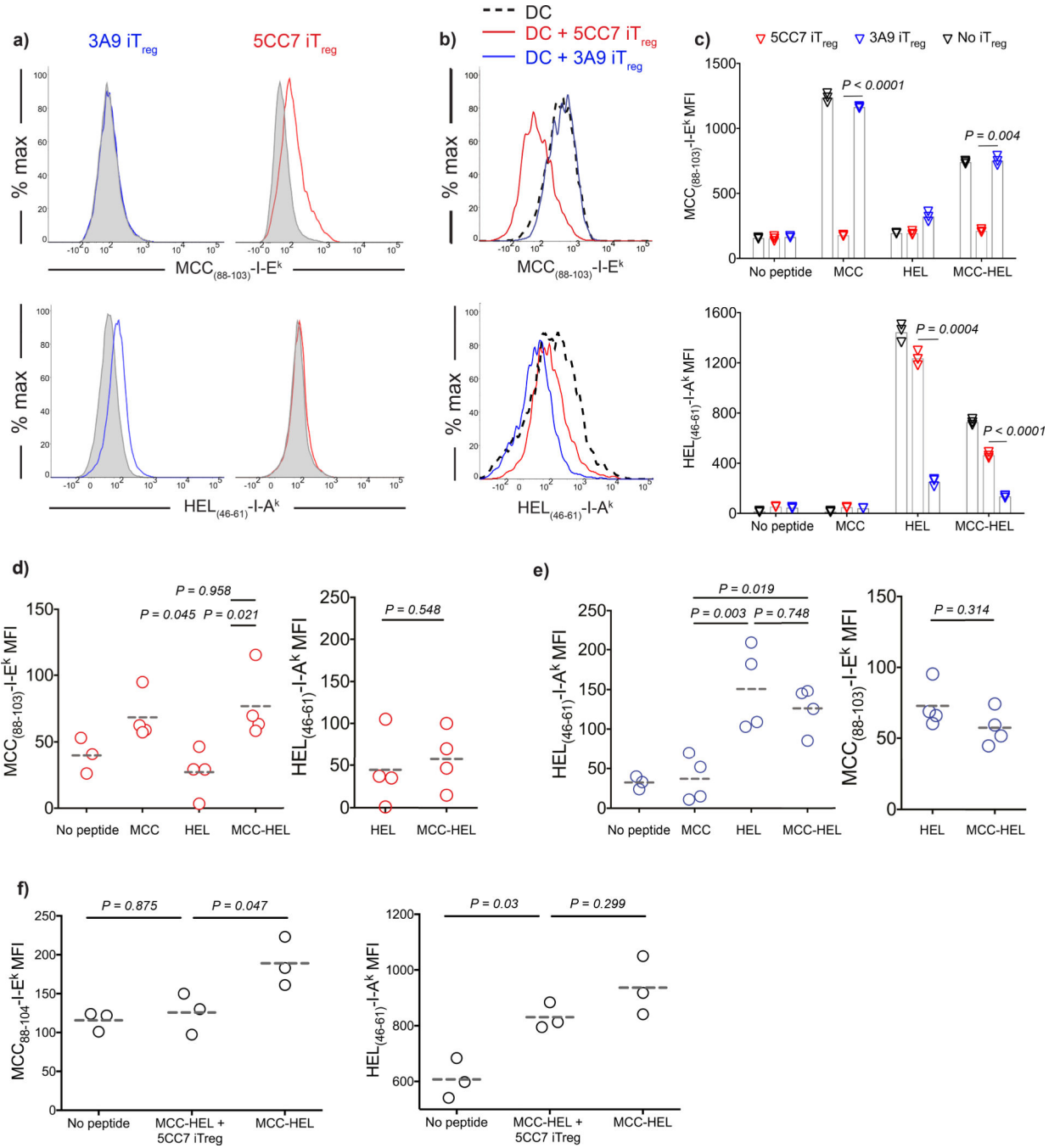
Figure 8:

Capture of pMHCII complexes by iT$_{regs}$ is antigen-specific. **a-c)** DCs were loaded with 3 μM MCC$_{(88-103)}$ and/or 3 μM HEL$_{(46-61)}$ and co-cultured 1:1 with 5CC7 or 3A9 iT$_{regs}$ for 18 h. **a)** Histograms demonstrate the MCC$_{(88-103)}$-I-E^k and HEL$_{(46-61)}$-I-A^k levels on 3A9 and 5CC7 iT$_{regs}$ co-cultured with double pulsed DCs (Red, blue) and unpulsed DC (Gray tinted). **b)** Histograms demonstrate the remaining MCC$_{(88-103)}$-I-E^k and HEL$_{(46-61)}$-I-A^k levels on double pulsed DCs after co-culture (Black dashed: Double antigen pulsed DC from solo culture. red: double pulsed DC co-cultured with 5CC7 iT$_{regs}$. blue: double pulsed DC

co-cultured with 3A9 iT$_{regs}$). **c)** Graphs show the levels for DC surface MCC$_{(88-103)}$-I-E^k and HEL$_{(46-61)}$-I-A^k. Bars indicate the mean of n=3 biological replicates and error bars represent the standard deviation. Data are representative of three independent experiments. **d-e)** Double pulsed DCs (5×10^4) were adoptively transferred into CD45.1$^+$B10A mice via the footpad together with e450 labeled 5CC7 or 3A9 iT$_{regs}$ (5×10^4) i.v. Day 3 post-transfer MFIs of iT$_{regs}$ for MCC$_{(88-103)}$-I-E^k (d) and HEL$_{(46-61)}$-I-A^k (e). Data are representative of three independent experiments, symbols show induvudual mice, lines mark the mean. **f)** DCs from B10.A animals were loaded with 3 μM MCC$_{(88-103)}$ and 3 μM HEL$_{(46-61)}$ or left unpulsed. DCs (1×10^6) and e450 labeled 5CC7 iT$_{regs}$ (1×10^6) were adoptively transferred into CD45.1$^+$B10A mice i.v. Graphs show the DC surface levels of pMHCII 18h post-transfer. Lines mark the mean of n=3 mice, data are representative of two independent experiments. *P* values were calculated using two-sided student's t-test (c) and one way ANOVA with Tukey's multiple comparison (d-f).